

A 125 GeV scalar improves the low-energy data support for the top-BESS model

Mikuláš Gintner^{1,2,*} and Josef Jurán^{2,3,†}

¹*Physics Department, University of Žilina, Univerzitná 1, 010 26 Žilina, Slovakia*

²*Institute of Experimental and Applied Physics, Czech Technical University in Prague,
Horská 3a/22, 128 00 Prague, Czech Republic*

³*Institute of Physics, Silesian University in Opava, Bezručovo nám. 13, 746 01 Opava, Czech Republic*

(Dated: November 1, 2018)

We investigate how adding a scalar resonance of a mass 125 GeV affects the low-energy data support for the top-BESS model as well as its low-energy free parameter limits. The top-BESS model is an effective Lagrangian, a modification of the well-known BESS model, with an ambition to describe phenomenology of the lowest bound states of strongly-interacting theories beyond the Standard model. In particular, the $SU(2)_{L+R}$ vector resonance triplet of hypothetical bound states is a centerpiece of BESS-like effective models. The top-BESS model assumes that the triplet couples directly to the third quark generation only. This assumption reflects a possible special standing of the third quark generation, and the top quark in particular, in physics of electroweak symmetry breaking. Our findings suggest that the 125 GeV scalar extension of the top-BESS model results in a higher statistical support for the model. The best-fit values of the model's free parameters are consistent with the top quark having a higher degree of compositeness than the bottom quark.

PACS numbers: 12.60.Fr, 12.39.Fe, 12.15.Ji

I. INTRODUCTION

Even though the ATLAS and CMS announcements of the 125 GeV boson discovery [1] have not settled the question about the mechanism of electroweak symmetry breaking yet they did provide major hints pointing to its solution. At the moment, it is clear that the observed properties of the discovered boson are compatible with the Standard model Higgs boson hypothesis [2–4]. At the same time they are compatible with many alternative extensions of the Standard model (SM). From a theoretical point of view, the extensions get some preference over the SM Higgs due to the naturalness argument. They include supersymmetry theories as well as theories where electroweak symmetry is broken by new strong interactions, like in Technicolor [5–8].

Most studies aimed at the evaluation of the impact of the new discovery on the alternative theories assume the boson has a spin zero [9] even though integer spins two and higher [10] are also admissible by the existing experimental evidence. Of course, this assumption disfavors strongly-interacting theories without light scalar fields and calls for theories with a light composite strongly-interacting Higgs [11] of a proper mass.

Following theoretical arguments, as well as the example of QCD, it seems reasonable to expect that beside the composite scalar the new strong interactions would also produce bound states of higher spins. The vector $SU(2)$ triplet resonance is a natural candidate to look for. From other point of view, in strongly interacting theories new resonances are required to tame the unitarity. If, as expected, the composite Higgs couplings differ

from the SM ones the Higgs alone will fail to unitarize the VV ($V = W^\pm, Z$) scattering amplitudes and other resonances are necessary to do the job.

The new scalar can be accommodated by extra-dimensional theories [12] as well. There, additional new resonances, if observed at the LHC, could be the lowest Kaluza-Klein excitations. The attractiveness of this development is strengthened by the Maldacena's conjecture [13] on the dual-description relation between the extra-dimensional weakly-interacting theories and the strongly-interacting models in four dimensions.

The effective field theory can describe low-energy physics of fundamental theories beyond the SM. In the case of strongly-interacting theories where the standard tools of perturbative field theory have limited applicability the effective field theory is a viable tool for the phenomenology of bound states. In addition, it can provide a unifying description of the low-energy phenomenologies of various new physics candidates and a useful bridge between theory and experiment. The BESS model [14] is an example of the effective Lagrangian describing the Higgsless ESB sector with an extra $SU(2)_{L+R}$ vector triplet.

Recently, we introduced and studied a modification of the BESS model, the top-BESS model [15]. The global $SU(2)_L \times SU(2)_R$ symmetry of both models is broken down to $SU(2)_{L+R}$. In these models, the vector resonance triplet is introduced as a gauge field via the hidden local symmetry approach [16]. Inspired by the speculations about a special role of the top quark (or the third quark generation) in the mechanism of ESB we modified the direct interactions of the vector triplet with fermions. While in the BESS model there is a universal direct coupling of the triplet to all fermions of a given chirality, in our modification we admit direct couplings of the new triplet to top and bottom quarks only.

In the strong scenario, the direct coupling between the

* gintner@fyzika.uniza.sk

† josef.juran@utef.cvut.cz

SM fermions and the vector resonance can depend on the degree of compositeness of a given fermion as well as on symmetry group representations the fermions are organized into. In principle, the degree of compositeness of the SM fermions can vary for different flavors and chirality. In addition, in some models the masses of the SM fermions are related to the product of compositeness of the left and right chirality [17–19]. If so, the hierarchy of the SM fermion masses provides a reasonable motivation to assume the third quark generation exclusivity regarding the direct interaction with the vector resonance triplet. On the other hand, universal degree of compositeness for all quarks is also viable [19].

In the top-BESS model, we allow for the possible chirality dependence of the direct triplet-to-top/bottom coupling. In addition, we admit disentanglement of the triplet-to-top-quark right coupling from the triplet-to-bottom-quark right coupling. This breaks the $SU(2)_R$ symmetry which is broken by the SM interactions, anyway. For the sake of the top-bottom disentanglement, we have introduced a free parameter p that can weaken, or even turn off, the strength of the triplet-to- b_R coupling by assuming its value between zero and one. However, the $SU(2)_L$ symmetry does not allow us to do the same splitting for the left quark doublet.

Originally, as the BESS model, the top-BESS model has been formulated without scalar resonances of any kind because the primary goal was the systematic effective description and study of a vector bound state physics. However, the discovery of the new boson motivates us to study the consequences of the inclusion of a 125-GeV scalar resonance into the top-BESS model. The inclusion of composite scalar resonance(s) into strongly interacting models were already considered in many papers [11], [19–22].

In this paper, we investigate how the inclusion of the 125-GeV scalar resonance influences the best fits of the top-BESS parameters to the existing low-energy data. This analysis have been performed as a multi-observable χ^2 -fit taking into account the correlations among the observables used. The list of fitted observables is comprised of ϵ_1 , ϵ_2 , ϵ_3 , ϵ_b when $p = 0$ and $\Gamma_b(Z \rightarrow b\bar{b} + X)$ otherwise, and $\text{BR}(B \rightarrow X_s \gamma)$. The mass of the considered vector triplet assumes TeV values. The top-BESS predictions of the observables are derived up to a 1-loop level within some approximations and after integrating out the vector resonance triplet.

The maximum number of fitting parameters is four: the vector resonance gauge coupling and three parameters, including p , responsible for the direct couplings of the vector resonances to the top and bottom quarks. We also perform fits when some of the parameters assume fixed values. Motivation for fixing the values can be theoretical. To simplify the analysis the free parameters of the scalar resonance are set to their SM values.

As a by-product, this paper contains an improved analysis of the low-energy limits of the top-BESS model without any scalar resonances in its spectrum. In the orig-

inal paper [15], the analogical analysis was based on a single-observable fits only. Besides, here we extend the epsilon analysis by adding the ϵ_2 parameter not considered in [15].

This paper is organized as follows. Section II is devoted to the formulation of the top-BESS model. In Subsection II A we briefly recall its original formulation as it has been done in [15]. Then, in Subsection II B the model is extended by adding a scalar field representing the 125-GeV scalar resonance. The low-energy χ^2 analysis is performed in Section III. Particularly, in Subsection III A we introduce observables that will be fitted and show their relation to the anomalous fermion couplings. In Subsection III B we provide the low-energy top-BESS expressions for the observables. The obtained best-fit values of the free parameters of the low-energy limit of the top-BESS model and their data support along with the corresponding confidence intervals are shown and discussed in several parts of Section IV. Conclusions are contained in Section V. There are three appendices in this paper. In Appendix A the experimental values of the observables we use in our analysis can be found. Appendix B is devoted to the low-energy top-BESS Lagrangian. Finally, Appendix C provides a very brief summary of the relations used in the χ^2 statistical analysis.

II. THE TOP-BESS MODEL

The top-BESS model was originally formulated without any new scalar fields [15]. In this section we will briefly recall its formulation. Then, we will extend the model by adding a scalar resonance with an ambition to accommodate the discovery of the 125-GeV boson.

A. Original formulation: no scalar resonance

In this subsection we briefly summarize the top-BESS effective Lagrangian as it was formulated in [15]. The Lagrangian possesses the $SU(2)_L \times SU(2)_R \times U(1)_{B-L} \times SU(2)_{HLS}$ global symmetry of which the $SU(2)_L \times U(1)_Y \times SU(2)_{HLS}$ subgroup is also a local symmetry. ‘HLS’ stands for the *hidden local symmetry* [16] which is an auxiliary gauge symmetry introduced to accommodate the $SU(2)$ triplet of vector resonances. Beside the triplet, the model contains only the observed SM particles.

The top-BESS effective Lagrangian can be split in three parts

$$\mathcal{L}_{\text{tBESS}} = \mathcal{L}_{\text{GB}} + \mathcal{L}_{\text{ESB}} + \mathcal{L}_{\text{ferm}}, \quad (1)$$

where \mathcal{L}_{GB} describes the gauge boson sector including the $SU(2)_{\text{HLS}}$ triplet, \mathcal{L}_{ESB} is the scalar sector responsible for spontaneous breaking of the electroweak and hidden local symmetries, and $\mathcal{L}_{\text{ferm}}$ is the fermion Lagrangian of the model.

In the gauge-boson sector, beside the SM gauge fields $W_\mu^a(x)$ and $B_\mu(x)$, there is the $SU(2)_{\text{HLS}}$ gauge triplet $\vec{V}_\mu = (V_\mu^1, V_\mu^2, V_\mu^3)$ introduced. Under the $[SU(2)_L \times SU(2)_R]^{\text{glob}} \times SU(2)_{\text{HLS}}^{\text{loc}}$ group it transforms as

$$\mathbf{V}_\mu \rightarrow h^\dagger \mathbf{V}_\mu h + h^\dagger \partial_\mu h, \quad (2)$$

where $h(x) \in SU(2)_{\text{HLS}}^{\text{loc}}$ and $\mathbf{V}_\mu = i\frac{g''}{2}V_\mu^a\tau^a$. The 2×2 matrices $\vec{\tau} = (\tau^1, \tau^2, \tau^3)$ are the $SU(2)$ generators.

The gauge boson Lagrangian \mathcal{L}_{GB} is composed of the Lagrangians for the individual gauge bosons

$$\mathcal{L}_W = \frac{1}{2g^2} \text{Tr}(\mathbf{W}_{\mu\nu} \mathbf{W}^{\mu\nu}), \quad (3)$$

$$\mathcal{L}_B = \frac{1}{2g'^2} \text{Tr}(\mathbf{B}_{\mu\nu} \mathbf{B}^{\mu\nu}), \quad (4)$$

$$\mathcal{L}_V = \frac{2}{g''^2} \text{Tr}(\mathbf{V}_{\mu\nu} \mathbf{V}^{\mu\nu}), \quad (5)$$

with the field strength tensors

$$\mathbf{W}_{\mu\nu} = \partial_\mu \mathbf{W}_\nu - \partial_\nu \mathbf{W}_\mu + [\mathbf{W}_\mu, \mathbf{W}_\nu], \quad (6)$$

$$\mathbf{B}_{\mu\nu} = \partial_\mu \mathbf{B}_\nu - \partial_\nu \mathbf{B}_\mu, \quad (7)$$

$$\mathbf{V}_{\mu\nu} = \partial_\mu \mathbf{V}_\nu - \partial_\nu \mathbf{V}_\mu + [\mathbf{V}_\mu, \mathbf{V}_\nu], \quad (8)$$

where $\mathbf{W}_\mu = igW_\mu^a\tau^a$, $\mathbf{B}_\mu = ig'B_\mu Y$ are $SU(2)_L$ and $U(1)_Y$ gauge fields.

The ESB sector contains six unphysical real scalar fields, would-be Goldstone bosons of the model's spontaneous symmetry breaking. Thus, naturally, the sector provides the energy scale v of ESB. The six real scalar fields $\varphi_L^a(x), \varphi_R^a(x)$, $a = 1, 2, 3$, are introduced as parameters of the $SU(2)_L \times SU(2)_R$ group elements in the exp-form $\xi(\vec{\varphi}_{L,R}) = \exp(i\vec{\varphi}_{L,R}\vec{\tau}/v) \in SU(2)_{L,R}$ where $\vec{\varphi} = (\varphi^1, \varphi^2, \varphi^3)$.

The scalar fields couple to the gauge bosons in the form given by the $[SU(2)_L \times U(1)_Y \times SU(2)_{\text{HLS}}]^{\text{loc}}$ invariant Lagrangian

$$\mathcal{L}_{\text{ESB}} = -v^2 \left[\text{Tr}(\bar{\omega}_\mu^\perp)^2 + \alpha \text{Tr}(\bar{\omega}_\mu^\parallel)^2 \right], \quad (9)$$

where α is a free parameter and $\bar{\omega}_\mu^{\parallel,\perp}$ are, respectively, $SU(2)_{L-R}$ and $SU(2)_{L+R}$ projections of the gauged Maurer-Cartan 1-form,

$$\bar{\omega}_\mu^\parallel = \omega_\mu^\parallel + \frac{1}{2} \left(\xi_L^\dagger \mathbf{W}_\mu \xi_L + \xi_R^\dagger \mathbf{B}_\mu \xi_R \right) - \mathbf{V}_\mu, \quad (10)$$

$$\bar{\omega}_\mu^\perp = \omega_\mu^\perp + \frac{1}{2} \left(\xi_L^\dagger \mathbf{W}_\mu \xi_L - \xi_R^\dagger \mathbf{B}_\mu \xi_R \right), \quad (11)$$

where $\omega_\mu^{\parallel,\perp} = (\xi_L^\dagger \partial_\mu \xi_L \pm \xi_R^\dagger \partial_\mu \xi_R)/2$.

All the six scalar fields can be transformed away by an appropriate gauge transformation. Namely, the scalar triplet $\vec{\sigma} = (\vec{\varphi}_L + \vec{\varphi}_R)/2$ can be gauged away by the $SU(2)_{\text{HLS}}^{\text{loc}}$ transformation $h(x) = \xi(\vec{\sigma})$, leaving us with the pseudo-scalar triplet $\vec{\pi} = (\vec{\varphi}_L - \vec{\varphi}_R)/2$. The gauge transformation turns the Lagrangian (9) into the gauged non-linear sigma model on the $SU(2)_L \times$

$SU(2)_R/SU(2)_{L+R}$ coset space. The triplet $\vec{\pi}$ plays a role of the Goldstone bosons which supply masses to the electroweak gauge bosons through the Higgs mechanism. The $SU(2)_{\text{HLS}}$ vector triplet enters the resulting non-linear sigma model Lagrangian in the way introduced originally by Weinberg [23].

The masses of the vector triplet depend on the three gauge couplings g, g', g'' , the free parameter α , and the ESB scale v . In the limit when g and g' are negligible compared to g'' the masses of the neutral and charged resonances are degenerate, $M_V = \sqrt{\alpha}g''v/2$. If higher order corrections in g/g'' are admitted a tiny mass splitting occurs such that $M_{V^0} > M_{V^\pm}$.

In the top-BESS model, the interactions of the new vector triplet with the SM fermions have been modified. No new fermions beyond the SM have been introduced. The modification singles out the new physics role of the third quark generation, and of the top quark in particular. Hence, the name the *top-BESS model*, or *tBESS* in short.

The top-BESS fermion Lagrangian can be split in three parts

$$\mathcal{L}_{\text{ferm}} = \mathcal{L}_{\text{ferm}}^{\text{SM}} + \mathcal{L}_{(t,b)}^{\text{tBESS}} + \mathcal{L}_{\text{mass}}, \quad (12)$$

where $\mathcal{L}_{\text{ferm}}^{\text{SM}}$ is the SM part and $\mathcal{L}_{(t,b)}^{\text{tBESS}}$ contains the modification concerning the third quark generation

$$\begin{aligned} \mathcal{L}_{(t,b)}^{\text{tBESS}} = & b_L [I_b^L(\psi_L) - I_c^L(\psi_L)] + b_R [I_b^R(P\psi_R) - I_c^R(P\psi_R)] \\ & + 2\lambda_L I_\lambda^L(\psi_L) + 2\lambda_R I_\lambda^R(P\psi_R), \end{aligned} \quad (13)$$

where $\psi = (t, b)$, and

$$I_c^L(\psi_L) = i\bar{\psi}_L(\not{\partial} + \not{\mathbf{W}} + \not{\mathbf{B}})\psi_L, \quad (14)$$

$$I_c^R(\psi_R) = i\bar{\psi}_R(\not{\partial} + \not{\mathbf{B}})\psi_R, \quad (15)$$

$$I_b^h(\psi_h) = i\bar{\chi}_h[\not{\partial} + \not{\mathbf{V}} + ig'\not{\mathbf{B}}(B-L)/2]\chi_h, \quad (16)$$

$$\begin{aligned} I_\lambda^h(\psi_h) = & i\bar{\chi}_h\vec{\varphi}^\perp\chi_h \\ = & i\bar{\chi}_h \left[\varphi^\perp + (\xi_L^\dagger \mathbf{W} \xi_L - \xi_R^\dagger \mathbf{B}^{R3} \xi_R)/2 \right] \chi_h, \end{aligned} \quad (17)$$

where $h = L, R$, $\mathbf{B}^{R3} = ig' \mathbf{B} \tau^3$, $\chi_h \equiv \chi(\vec{\varphi}_h, \psi_h) = \xi^\dagger(\vec{\varphi}_h) \cdot \psi_h$. The matrix $P = \text{diag}(1, p)$ serves to disentangle the direct interaction of the vector triplet with the right top quark from the interaction with the right bottom quark. While $p = 1$ leaves the interactions equal, the $p = 0$ turns off the right bottom quark interaction completely and maximally breaks the $SU(2)_R$ part of the Lagrangian symmetry down to $U(1)_{R3}$.

The fermion masses are encoded in the Lagrangian term $\mathcal{L}_{\text{mass}} = -\sum_i I_{\text{mass}}(\psi^i)$ where the sum runs over all SM fermion doublets and

$$I_{\text{mass}}(\psi^i) = \bar{\psi}_L^i U M_f^i \psi_R^i + \text{H.c.}, \quad (18)$$

where M_f^i is a 2×2 diagonal matrix with the masses of the upper and bottom fermion doublet components on its diagonal, and $U = \xi(\vec{\pi}) \cdot \xi(\vec{\pi}) = \exp(2i\vec{\pi}\vec{\tau}/v)$.

In the unitary (physical) gauge where all six unphysical scalar fields are gauged away the gauged MC 1-form projections (10) and (11) read

$$\bar{\omega}_{\perp,\mu} = \frac{1}{2}(\mathbf{W}_\mu - \mathbf{B}_\mu), \quad (19)$$

$$\bar{\omega}_{\parallel,\mu} = \frac{1}{2}(\mathbf{W}_\mu + \mathbf{B}_\mu) - \mathbf{V}_\mu, \quad (20)$$

and the new physics part of the (t, b) Lagrangian assumes the form

$$\begin{aligned} \mathcal{L}_{(t,b)}^{\text{tBESS}} = & ib_L \bar{\psi}_L (\mathbf{V} - \mathbf{W}) \psi_L + ib_R \bar{\psi}_R (\mathbf{V} - \mathbf{B}^{R3}) \psi_R \\ & + i \sum_{h=L,R} \lambda_h \bar{\psi}_h (\mathbf{W} - \mathbf{B}^{R3}) \psi_h. \end{aligned} \quad (21)$$

Once the gauge boson fields are expressed in the mass eigenstate basis the mixing generated interactions of the vector triplet with all fermions will appear on the scene. However, these indirect interactions with the light fermions will be suppressed by the mixing matrix elements proportional to $1/g''$.

B. Adding a scalar resonance

The recent discovery of the 125 GeV boson [1] motivates considerations about possible extensions of the top-BESS model. The focus of the pre-discovery formulation of the top-BESS model [15] lain in the study of the new physics vector resonance. To avoid unnecessary complications the model's Lagrangian did not contain any other non-SM fields. Now, however, the model has to face the facts about the new 125-GeV boson.

We have chosen to investigate the simplest possibility: the extension of the top-BESS model by the neutral scalar isoscalar resonance field $h(x)$ of the mass $M_h = 125$ GeV. Since the transformation properties of such a field under the model's symmetry group are trivial it is not difficult to build additional Lagrangian terms to the top-BESS effective Lagrangian (see, e.g., [2, 19, 21]).

Adding the scalar to the top-BESS model can result in the following modifications of the original Lagrangian (1)

$$\mathcal{L}_{\text{ESB}} \rightarrow \mathcal{L}_{\text{ESB}} \times (1 + 2a \frac{h}{v} + a' \frac{h^2}{v^2} + \dots), \quad (22)$$

$$I_{\text{mass}}(\psi^i) \rightarrow I_{\text{mass}}(\psi^i) \times (1 + c_i \frac{h}{v} + c'_i \frac{h^2}{v^2} + \dots), \quad (23)$$

where a, a', \dots and c_i, c'_i, \dots are free parameters. Note that the modifications maintain the custodial symmetry. The a and c parameters parameterize deviations of the h couplings to the massive electroweak gauge bosons and to fermions, respectively, from those of the SM Higgs boson. Indeed, when $a = a' = c_i = 1, \forall i$, and the rest are zeros the scalar resonance imitates the SM Higgs boson. Of course, the mass and kinetic terms for the scalar resonance are needed. The self-interactions of the scalar particle can be introduced as well.

The part of the effective Lagrangian relevant to LHC phenomenology includes linear couplings of the scalar to SM particles and to the vector resonance [19]. In addition, in the top-BESS model, we will assume the flavor universality, $c_i \equiv c, \forall i$. Then, in the unitary gauge, the top-BESS Lagrangian with the 125 GeV scalar resonance reads

$$\begin{aligned} \tilde{\mathcal{L}}_{\text{tBESS}} = & \mathcal{L}_{\text{tBESS}} + \frac{1}{2} \partial_\mu h \partial^\mu h - \frac{1}{2} M_h^2 h^2 \\ & + a \left(\frac{2M_W^2}{v} W_\mu^+ W^{-\mu} + \frac{M_Z^2}{v} Z_\mu Z^\mu \right. \\ & \quad \left. + \frac{2M_{V^\pm}^2}{v} V_\mu^+ V^{-\mu} + \frac{M_{V^0}^2}{v} V_\mu^0 V^{0\mu} \right) h \\ & - \sum_f c \frac{m_f}{v} (\bar{f}_L f_R + \text{H.c.}) h, \end{aligned} \quad (24)$$

where $\mathcal{L}_{\text{tBESS}}$ is the original top-BESS Lagrangian and m_f stands for the fermion masses. The interactions of the scalar resonance with all gauge fields are parametrized by the same parameter a . The couplings of the scalar resonance to the SM fermions are parameterized by c .

The constraints on the deviations a and c [2] resulting from the global analysis of the available CMS, ATLAS, CDF, and D0 data are consistent with the 125-GeV SM Higgs boson. Therefore, in this paper we opt for $a = c = 1$ and focus on the simplified task of fitting the vector resonance related free parameters only.

The presence of the scalar resonance in the top-BESS particle spectrum also affects the unitarity bounds. For the higgsless case we have calculated such theoretical unitarity constraints in [15]. As one might have expected the inclusion of the scalar resonance can significantly relax the unitarity constraints [19]. Of course, the more closer the parameter a is to one the more relaxed the unitarity constraints are.

III. THE LOW-ENERGY ANALYSIS

In this section we are going to perform a multi-observable fit of (pseudo)observables¹ $\epsilon_1, \epsilon_2, \epsilon_3, \epsilon_b$ or $\Gamma_b(Z \rightarrow b\bar{b})$, and $\text{BR}(B \rightarrow X_s \gamma)$ by the top-BESS parameters. We will study the influence of the 125 GeV scalar resonance on the best-fit values of the parameters and on their statistical support. As far as the observables are concerned the inclusion of the scalar resonance will affect loop-level contributions to the epsilons.

¹ The quantities Γ_b and $\text{BR}(B \rightarrow X_s \gamma)$ are more intimately related to actual observables than the epsilons. To stress this fact one might wish to nickname the epsilons as *pseudo-observables*. Nevertheless, in the following text we will not make this distinction and will rather call the epsilons as observables, too.

A. (Pseudo)observables

The epsilons are related to the *basic observables* [24]: the ratio of the electroweak gauge boson masses, $r_M \equiv M_W/M_Z$; the inclusive partial decay width of Z to the charged leptons, $\Gamma_\ell(Z \rightarrow \ell\bar{\ell} + \text{photons})$; the forward-backward asymmetry of charged leptons at the Z -pole, $A_\ell^{FB}(M_Z)$; and the inclusive partial decay width of Z to bottom quarks, $\Gamma_b(Z \rightarrow b\bar{b} + X)$.

The introduction of the scalar resonance to the top-BESS model Lagrangian does not affect the vector resonance equation of motion. Thus, the low-energy Lagrangian obtained after integrating out the vector resonance in (24) differs from the higgsless top-BESS low-energy Lagrangian by the terms responsible for the interactions of the scalar resonance with the SM fields only.

The deviations of r_M , Γ_ℓ , and A_ℓ^{FB} from their predicted SM tree level values including the QED and QCD loop contributions are parameterized by the *dynamical corrections* Δr_W , $\Delta\rho$, and Δk as follows [24]

$$(1 - r_M^2) r_M^2 = \frac{\pi\alpha(M_Z)}{\sqrt{2}G_F M_Z^2 (1 - \Delta r_W)} \quad (25)$$

and

$$\Gamma_\ell = \frac{G_F M_Z^3}{6\pi\sqrt{2}} (g_A^\ell)^2 (1 + r_g^2) \left(1 + \frac{3\alpha}{4\pi}\right), \quad (26)$$

$$A_\ell^{FB} = \frac{3r_g^2}{(1 + r_g^2)^2}, \quad (27)$$

where

$$g_A^\ell = -\frac{1}{2} \left(1 + \frac{\Delta\rho}{2}\right), \quad r_g = \frac{g_V^\ell}{g_A^\ell} = 1 - 4(1 + \Delta k)s_0^2. \quad (28)$$

The first three epsilons are defined as the combinations of the dynamical corrections [24]

$$\epsilon_1 = \Delta\rho, \quad (29)$$

$$\epsilon_2 = c_0^2 \Delta\rho + \frac{s_0^2}{c_{20}} \Delta r_W - 2s_0^2 \Delta k, \quad (30)$$

$$\epsilon_3 = c_0^2 \Delta\rho + c_{20} \Delta k, \quad (31)$$

where s_0 (c_0) is the sine (cosine) of the Weinberg angle, $c_{20} \equiv c_0^2 - s_0^2$. The value of s_0 depends on the values of $e(M_Z)$, G_F , and M_Z through the defining relation

$$s_0^2 c_0^2 \equiv \frac{\pi \alpha(M_Z)}{\sqrt{2} G_F M_Z^2}. \quad (32)$$

Given the experimental values of $\alpha(M_Z)$, M_Z , and G_F , s_0 can be considered as a replacement of G_F in this list. With this substitution the relation (25) can be rewritten in a simpler form

$$(1 - r_M^2) r_M^2 = \frac{s_0^2 c_0^2}{1 - \Delta r_W}. \quad (33)$$

Both, the dynamical corrections and the epsilon parameters were defined to assume zero values when the SM tree-level contributions along with the QED and QCD loop contributions are considered only. The SM weak loop corrections unzero the epsilon values.

The $Zb\bar{b}$ vertex is naturally tested in the $Z \rightarrow b\bar{b} + X$ decay. The corresponding decay width formula reads [24]

$$\Gamma_b = \frac{G_F M_Z^3}{6\pi\sqrt{2}} \beta \left[\frac{3 - \beta^2}{2} (g_V^b)^2 + \beta^2 (g_A^b)^2 \right] \times N_C R_{\text{QCD}} \left(1 + \frac{\alpha}{12\pi}\right), \quad (34)$$

where $\beta = (1 - 4m_b^2/M_Z^2)^{1/2}$, and $R_{\text{QCD}} = 1 + 1.2a - 1.1a^2 - 13a^3$ is the QCD correction factor, $a = \alpha_s(M_Z)/\pi$.

The precise measurement of Γ_b can uncover whether the bottom quark anomalous couplings $g_{V,A}^b$ differ from the anomalous couplings of other charged SM fermions. Assuming the couplings differ in their $SU(2)_L$ parts only the standard parameterization of the difference is by introducing the parameter ϵ_b [24]

$$g_A^b = g_A^\ell (1 + \epsilon_b), \quad (35)$$

$$g_V^b = \left(1 + \frac{\Delta\rho}{2}\right) \left[-\frac{1}{2}(1 + \epsilon_b) + \frac{2}{3}(1 + \Delta k)s_0^2\right]. \quad (36)$$

Thus, ϵ_b along with ϵ_1 , ϵ_2 , and ϵ_3 can be used to store the experimental information obtained by measuring the basic observables. Then, the experimental values of the epsilons can face predictions by a specific theory in order to transfer the information to the parameters of the theory.

However, the top-BESS effective Lagrangian admits a more general pattern of the bottom versus light quark anomalous coupling difference than it is assumed in the definition of ϵ_b . Within the top-BESS model the definition's assumptions are met when either $p = 0$, or $b_R = -2\lambda_R$. Otherwise, the experimental value of Γ_b rather than ϵ_b^{exp} must be related to the top-BESS theoretical prediction in order to derive the low-energy limits on the top-BESS free parameters.

The deviations from the SM can be related to the anomalous fermion weak couplings κ of the fermion interaction Lagrangian

$$\begin{aligned} \mathcal{L}_{\text{ferm.int.}}^{\text{anom}} = & -e\bar{\psi} A Q \psi - \frac{e}{\sqrt{2}s_0} \bar{\psi} (W^+ \tau^+ + W^- \tau^-) \times \\ & [(1 + \kappa_L^{Wf_u f_d}) P_L + \kappa_R^{Wf_u f_d} P_R] \psi \\ & - \frac{e}{2s_0 c_0} \bar{\psi} Z (K_L P_L + K_R P_R) \psi, \end{aligned} \quad (37)$$

where

$$K_L = 2(T_L^3 - s_0^2 Q) + \text{diag}(\kappa_L^{Zf_u f_u}, \kappa_L^{Zf_d f_d}), \quad (38)$$

$$K_R = -2s_0^2 Q + \text{diag}(\kappa_R^{Zf_u f_u}, \kappa_R^{Zf_d f_d}), \quad (39)$$

and the superscript f_u (f_d) indicates the upper (lower) component of any of the fermion doublets. The expressions (26), (27), and (34) result from

$$\kappa_L^{Z\ell\ell} = -\frac{\Delta\rho}{2} + 2s_0^2 \left[\frac{\Delta\rho}{2} + \Delta k \left(1 + \frac{\Delta\rho}{2}\right) \right], \quad (40)$$

$$\kappa_R^{Z\ell\ell} = 2s_0^2 \left[\frac{\Delta\rho}{2} + \Delta k \left(1 + \frac{\Delta\rho}{2} \right) \right], \quad (41)$$

$$\kappa_L^{Zbb} = g_V^b + g_A^b + 1 - \frac{2}{3}s_0^2, \quad (42)$$

$$\kappa_R^{Zbb} = g_V^b - g_A^b - \frac{2}{3}s_0^2. \quad (43)$$

In the case when the ϵ_b assumptions hold

$$\begin{aligned} \kappa_L^{Zbb} &= -\frac{\Delta\rho}{2}(1 + \epsilon_b) - \epsilon_b \\ &\quad + \frac{2}{3}s_0^2 \left[\frac{\Delta\rho}{2} + \Delta k \left(1 + \frac{\Delta\rho}{2} \right) \right], \end{aligned} \quad (44)$$

$$\kappa_R^{Zbb} = \frac{1}{3}\kappa_R^{Z\ell\ell}. \quad (45)$$

The $B \rightarrow X_s \gamma$ decay puts limits on the anomalous $W^\pm t_L b_L$ and $W^\pm t_R b_R$ vertices [25, 26]. In the SM it proceeds through the flavor changing neutral current loop process $b \rightarrow s \gamma$ dominated by the top quark exchange diagram. The $B \rightarrow X_s \gamma$ branching fraction can be sensitive to physics beyond the SM via new particles entering the penguin loop. When expressed in terms of the real anomalous Wtb couplings, κ_L^{Wtb} and κ_R^{Wtb} , it can be approximated by the following formula [26]

$$\begin{aligned} \text{BR}(B \rightarrow X_s \gamma) \times 10^4 &= 3.07 + 280 \kappa_R^{Wtb} + 2 \kappa_L^{Wtb} \\ &\quad + 5520 (\kappa_R^{Wtb})^2 + 0.3 (\kappa_L^{Wtb})^2 \\ &\quad + 79 \kappa_L^{Wtb} \kappa_R^{Wtb}. \end{aligned} \quad (46)$$

The experimental values of the observables used to derive the low-energy limits on the top-BESS free parameters can be found in Appendix A.

B. Top-BESS predictions

To derive the low-energy limits and the best-fit values of the top-BESS free parameters we have to obtain the top-BESS expressions for the observables. The expressions will be used to fit the experimental values of the observables. Since the values originate from measurements performed far below the considered vector resonance mass, $M_V = \mathcal{O}(\text{TeV})$, we can work within the framework of the low-energy limit of the top-BESS Lagrangian obtained by integrating out the $SU(2)_{\text{HLS}}$ vector triplet.

The predictions of the low-energy top-BESS (LE-tBESS) Lagrangian will be expressed in terms of the LE-tBESS input parameters $\{e, s_\theta, x, M_Z, \Delta L, \Delta R, p, \{m_f\}\}$ introduced in Appendix B along with the LE-tBESS Lagrangian itself.

The tree-level LE-tBESS contribution to the anomalous couplings of the light fermions f read (see Appendix B)

$$\kappa_L^{Wfufd} = h(x; s_0) - 1, \quad \kappa_R^{Wfufd} = 0, \quad (47)$$

$$\kappa_L^{Zff} = \kappa_R^{Zff} = -2s_0^2 \Delta k^{\text{LE}}(x; s_0) Q_f, \quad (48)$$

where

$$h(x; s_0) = \frac{s_0}{s_\theta} \sqrt{\frac{1 + 4s_\theta^2 x^2}{1 + x^2}} \quad (49)$$

and

$$\Delta k^{\text{LE}}(x; s_0) = \left(\frac{s_\theta}{s_0} \right)^2 \frac{1 + 2x^2}{1 + 4s_\theta^2 x^2} - 1. \quad (50)$$

Recall that $x = g/g''$ is a free parameter of the LE-tBESS Lagrangian (see the Eqs. (B4) and (B5)). Also note that

$$h(x; s_0) = 1 - s_0^2 \Delta k^{\text{LE}}(x; s_0) + \mathcal{O}(x^4) \quad (51)$$

$$= 1 - 0.430 x^2 - 0.405 x^4 + \dots \quad (52)$$

In the case of the top and bottom quarks the charged current tree-level LE-tBESS anomalous couplings read

$$\kappa_L^{Wtb} = h(x; s_0) \left(1 - \frac{\Delta L}{2} \right) - 1, \quad (53)$$

$$\kappa_R^{Wtb} = h(x; s_0) \frac{p \Delta R}{2}, \quad (54)$$

where the free parameters $\Delta L = b_L - 2\lambda_L$ and $\Delta R = b_R + 2\lambda_R$ parameterize the top and bottom quark couplings of the LE-tBESS Lagrangian (see the Eqs. (B16) – (B18) and (B24)). The neutral current tree-level LE-tBESS anomalous couplings read ($f = t, b$)

$$\kappa_L^{Zff} = -\Delta L T_L^3(f) - 2s_0^2 \Delta k^{\text{LE}}(x; s_0) Q_f, \quad (55)$$

$$\kappa_R^{Zff} = \Delta R P_f T_R^3(f) - 2s_0^2 \Delta k^{\text{LE}}(x; s_0) Q_f, \quad (56)$$

where $P_t = 1$, $P_b = p^2$. Breaking down the compact expressions (55) and (56) results in

$$\kappa_L^{Ztt} = -\frac{1}{2}\Delta L - \frac{4}{3}s_0^2 \Delta k^{\text{LE}}(x; s_0),$$

$$\kappa_R^{Ztt} = +\frac{1}{2}\Delta R - \frac{4}{3}s_0^2 \Delta k^{\text{LE}}(x; s_0),$$

$$\kappa_L^{Zbb} = +\frac{1}{2}\Delta L + \frac{2}{3}s_0^2 \Delta k^{\text{LE}}(x; s_0),$$

$$\kappa_R^{Zbb} = -\frac{p^2}{2}\Delta R + \frac{2}{3}s_0^2 \Delta k^{\text{LE}}(x; s_0).$$

By comparing the generic anomalous couplings (40) through (43) with the relevant tree-level LE-tBESS anomalous couplings for $f = \ell$ in (48), and for $f = b$ in (55), (56), the tree-level contributions to the dynamical corrections $\Delta\rho$ and Δk as well as to the bottom quark vector and axial-vector couplings $g_{V,A}^b$ can be obtained

$$(\Delta\rho)^{\text{LE}(0)} = 0, \quad (57)$$

$$(\Delta k)^{\text{LE}(0)} = \Delta k^{\text{LE}}, \quad (58)$$

$$(g_V^b)^{\text{LE}(0)} = \frac{1}{4}(\Delta L - p^2 \Delta R) + \frac{2}{3}\Delta k^{\text{LE}} s_0^2, \quad (59)$$

$$(g_A^b)^{\text{LE}(0)} = \frac{1}{4}(\Delta L + p^2 \Delta R). \quad (60)$$

The superscript LE(0) denotes contributions of the LE-tBESS at tree level. Of course, by definition, only the deviations from the corresponding SM terms can contribute non-trivially to the dynamical corrections and to the epsilons.

In addition, the tree-level contribution to Δr_W is obtained when the ratio $r_M^2 = (M_W/M_Z)^2$ expressed in terms of the LE-tBESS parameters as (see Appendix B)

$$r_M^2 = \frac{c_\theta^2 + x^2}{(1 + 4s_\theta^2 x^2)(1 + x^2)} \quad (61)$$

is substituted to the Eq. (33). Then

$$(\Delta r_W)^{\text{LE}(0)} = 1 - \left(\frac{1 + x^2}{1 + 2x^2} \right)^2. \quad (62)$$

Recall that the dynamical corrections $\Delta\rho$ and Δk can be expressed in terms of the epsilon parameters when inverting the Eqs. (29) through (31). The tree-level contributions $\epsilon_i^{\text{LE}(0)}$ for $i = 1, 2, 3$ can be obtained from the tree-level contributions to the dynamical corrections (57), (58), and (62). If $p = 0$ or $\Delta R = 0$, then $\epsilon_b^{\text{LE}(0)}$ can be obtained by comparing the expression (60) with the Eq. (35)

$$\epsilon_b^{\text{LE}(0)} = -\frac{1}{2}\Delta L. \quad (63)$$

Otherwise, the expressions (59) and (60) are used to calculate the LE-tBESS tree-level value of Γ_b , employing (34).

Using the numerical values shown in Appendix A the tree-level contributions to ϵ_i , $i = 1, 2, 3$, can be expressed as functions of x

$$\begin{aligned} \epsilon_1^{\text{LE}(0)} &= 0, \\ \epsilon_2^{\text{LE}(0)} &= \frac{s_0^2}{c_{20}} \frac{x^2(2 + 3x^2)}{(1 + 2x^2)^2} - 2s_0^2 \Delta k^{\text{LE}}, \\ \epsilon_3^{\text{LE}(0)} &= c_{20} \Delta k^{\text{LE}}. \end{aligned}$$

Their power series read

$$\epsilon_2^{\text{LE}(0)} = -2.71 x^4 + 2.96 x^6 + \dots, \quad (64)$$

$$\epsilon_3^{\text{LE}(0)} = x^2 + 0.66 x^4 + 2.56 x^6 + \dots \quad (65)$$

There is no reason to expect that the LE-tBESS anomalies at the tree level overwhelm the 1-loop contributions of the LE-tBESS model to the epsilons. Thus, both contributions should be considered when predicting the epsilon observables

$$\epsilon_i^{\text{LE}} = \epsilon_i^{\text{LE}(0)} + \epsilon_i^{\text{LE}(1)}, \quad i = 1, 2, 3, b, \quad (66)$$

where LE(1) denotes the 1-loop contributions of the LE-tBESS model.

Since we study an effective non-renormalizable Lagrangian it is not that obvious how to properly deal with the higher order calculations [25]. One does not know the

underlying theory therefore there is no way to establish a correct scheme for the effective Lagrangian [27]. While the divergent piece in loop calculations can be associated with a physical cutoff Λ up to which the effective Lagrangian is valid [28], for the finite piece there is no completely satisfactory approach available [29].

Beside the deviations in the fermion couplings of the gauge bosons represented by the kappas, deviations from the SM in the Higgs sector should contribute to the epsilons as well. The Higgs sector of the scalar-less case is represented by the gauged non-linear sigma model that can be viewed as the $M_H \rightarrow \infty$ limit of the SM Higgs sector. In this case, we approximate $\epsilon_i^{\text{LE}(1)}$ by the sum of the SM weak loop corrections $\epsilon_i^{\text{SM}(1)}$ and the loop contributions $\epsilon_i^{\kappa(1)}$ due to the kappas in the anomalous fermion Lagrangian (37)

$$\epsilon_i^{\text{LE}(1)} \approx \epsilon_i^{\text{SM}(1)} + \epsilon_i^{\kappa(1)}. \quad (67)$$

Of course, the SM(1) contributions depend on the mass of the non-existing SM Higgs boson. Thus, M_H is just a free tuning parameter of the approximation. We set it to the value of the cut-off scale Λ_{LE} of the LE-tBESS Lagrangian. The cut-off scale Λ_{LE} , in turn, can be identified with the mass of the integrated-out vector resonance.

In the 125-GeV scalar case, the first term of the approximation (67) should be replaced by the loop contributions due to the anomalous couplings of the scalar resonance to the gauge bosons and to fermions. However, since we assume that the scalar has the Higgs-like couplings we end up with $\epsilon_i^{\text{SM}(1)}$ again. This time though M_H represents the mass of the scalar resonance and should be set to 125 GeV.

To cover both possibilities — no scalar as well as the 125-GeV scalar resonance — the 1-loop SM contributions have been evaluated for four different values of M_H . The 125 GeV value corresponds to the case when a new scalar resonance imitating the LHC discovery is added to the spectrum of the top-BESS model; 300 GeV, 1 TeV, and 2 TeV values correspond to the top-BESS model without a scalar resonance.

The 1-loop SM contributions to the epsilon parameters are given by the following relations [30]

$$\epsilon_1^{\text{SM}(1)} = \left(+5.60 - 0.86 \ln \frac{M_H}{M_Z} \right) \times 10^{-3}, \quad (68)$$

$$\epsilon_2^{\text{SM}(1)} = \left(-7.09 + 0.16 \ln \frac{M_H}{M_Z} \right) \times 10^{-3}, \quad (69)$$

$$\epsilon_3^{\text{SM}(1)} = \left(+5.25 + 0.54 \ln \frac{M_H}{M_Z} \right) \times 10^{-3}, \quad (70)$$

$$\epsilon_b^{\text{SM}(1)} = -6.43 \times 10^{-3}. \quad (71)$$

The numerical values of $\epsilon_i^{\text{SM}(1)}$ for the quoted values of M_H are shown in Table I.

The 1-loop SM contributions to g_V^b and g_A^b can be obtained subtracting the SM tree-level couplings from the

TABLE I. The values of the SM 1-loop contributions to the epsilon parameters considering four different masses of the SM Higgs boson: 125 GeV, 300 GeV, 1 TeV, and 2 TeV.

M_H (GeV)	125	300	1000	2000
$\epsilon_1^{\text{SM}(1)} \times 10^3$	5.33	4.58	3.54	2.94
$\epsilon_2^{\text{SM}(1)} \times 10^3$	-7.04	-6.90	-6.71	-6.60
$\epsilon_3^{\text{SM}(1)} \times 10^3$	5.42	5.89	6.54	6.92
$\epsilon_b^{\text{SM}(1)} \times 10^3$	-6.43	-6.43	-6.43	-6.43

SM tree plus 1-loop couplings

$$(g_{V,A}^b)^{\text{SM}(1)} = (g_{V,A}^b)^{\text{SM}(0+1)} - (g_{V,A}^b)^{\text{SM}(0)}, \quad (72)$$

where $(g_{V,A}^b)^{\text{SM}(0+1)}$ are given by the Eqs. (35) and (36) if $\Delta\rho = (\Delta\rho)^{\text{SM}(1)}$, $\Delta k = (\Delta k)^{\text{SM}(1)}$, and $\epsilon_b = \epsilon_b^{\text{SM}(1)}$ are applied. Of course, $(g_V^b)^{\text{SM}(0)} = -1/2 + 2s_0^2/3$ and $(g_A^b)^{\text{SM}(0)} = -1/2$.

The $\epsilon_i^{\kappa(1)}$ contributions can be calculated using the results of [26]. In the context of the non-linear electroweak chiral Lagrangian the paper provides expressions for new physics loop contributions to the epsilon parameters in terms of generic anomalous couplings of the Lagrangian (37). Up to the order of $m_t^2 \ln \Lambda^2$ the anomalous loop contributions read [26]

$$\epsilon_1^{\text{NP}(1)} = \frac{3m_t^2 G_F}{2\sqrt{2}\pi^2} \ln \frac{\Lambda^2}{m_t^2} [\kappa_L^{Wtb} (1 + \kappa_L^{Wtb}) + (\kappa_R^{Ztt} - \kappa_L^{Ztt}) (1 - \kappa_R^{Ztt} + \kappa_L^{Ztt})], \quad (73)$$

$$\epsilon_2^{\text{NP}(1)} = \epsilon_3^{\text{NP}(1)} = 0, \quad (74)$$

$$\epsilon_b^{\text{NP}(1)} = \frac{m_t^2 G_F}{2\sqrt{2}\pi^2} \ln \frac{\Lambda^2}{m_t^2} \times \left[\left(\kappa_L^{Ztt} - \frac{1}{4} \kappa_R^{Ztt} \right) (1 + 2\kappa_L^{Wtb}) \right], \quad (75)$$

where Λ is the cut-off scale of the effective Lagrangian under consideration. In the cases when the NP(1) contributions depend on κ^{Zbb} the dependence is suppressed by $m_b \ll m_t$.

To obtain $\epsilon_1^{\kappa(1)}$ and $\epsilon_b^{\kappa(1)}$ one has to substitute the LE-tBESS anomalous couplings (53) – (56) into the expressions above. The cut-off scale of the LE-tBESS Lagrangian has been set to the mass of the integrated-out vector resonance, $\Lambda = \Lambda_{\text{LE}} = M_V$. When $M_V = 1$ TeV and using the numerical values of Appendix A the leading terms of the x^2 series of $\epsilon_1^{\kappa(1)}$ and $\epsilon_b^{\kappa(1)}$ read

$$\frac{\epsilon_1^{\kappa(1)}}{10^{-2}} = 6.57 \Delta R - 2.82 (2 - 3 \Delta L) x^2 + \dots, \quad (76)$$

$$\frac{\epsilon_b^{\kappa(1)}}{10^{-2}} = -0.55 (4 \Delta L + \Delta R) - (1.88 - 0.47 \Delta R - 3.76 \Delta L) x^2 + \dots, \quad (77)$$

where we have also neglected non-linear terms in ΔL , ΔR . The $\epsilon_1^{\kappa(1)}$ and $\epsilon_b^{\kappa(1)}$ series for $M_V = 0.3$ TeV and

$M_V = 2$ TeV are obtained when multiplying (76) and (77) by the numerical factors of 0.31 and 1.39, respectively.

In our analysis, we have not calculated $(g_{V,A}^b)^{\kappa(1)}$. Thus, the fit when $p \neq 0$ is based on the LE(0) and SM(1) contributions to $g_{V,A}^b$ only. We justified this simplifying approximation by comparing the single-observable fits based on $\epsilon_b^{\text{LE}(0)+\text{SM}(1)+\kappa(1)}$ with the fits based on $(g_{V,A}^b)^{\text{LE}(0)+\text{SM}(1)}$ when $p = 0$, see [15]. Fig. 11 of [15] illustrates that the absence of the $\kappa(1)$ contribution in the latter fits introduces only relatively small shifts in the obtained confidence level contours.

The LE-tBESS prediction of $\text{BR}(B \rightarrow X_s \gamma)$ has been calculated by substituting (53) and (54) into (46).

IV. RESULTS

Using the exact formulas for the LE-tBESS predictions we have performed a multi-parameter χ^2 fit of the observables in order to obtain the most preferred values and confidence level intervals for the LE-tBESS parameters. Two slightly different sets of observables have been fitted. The first set of fitted observables consists of $\{\epsilon_1, \epsilon_2, \epsilon_3, \epsilon_b, \text{BR}(B \rightarrow X_s \gamma)\} \equiv \text{Set-A}$. The fit of the Set-A has been used to investigate the low-energy data support for the top-BESS model when the vector resonance does not couple to the right bottom quark, i.e. $p = 0$. The second set of fitted observables consists of $\{\epsilon_1, \epsilon_2, \epsilon_3, \Gamma_b, \text{BR}(B \rightarrow X_s \gamma)\} \equiv \text{Set-B}$. In the fit of the Set-B, p can assume non-zero values and it can be one of the free fitting parameters of the top-BESS model. The experimental values of the observables are shown in Appendix A. The basic χ^2 -fit relations used in our calculations are summarized in Appendix C.

A. Single- vs. multi-observable fits

In [15] we have derived the limits on the top-BESS parameters as the intersections of various single-observable fits. Here, we perform comparison with the multi-observable fit results based on the same observables.

We start by restricting the LE-tBESS parameter x . Since g'' is a function² of x , this translates into limits on the most fundamental of the top-BESS free parameters: the $SU(2)_{\text{HLS}}$ gauge coupling g'' . The physically sensible values of g'' are bounded from below by the unitarity limits and from above by the perturbativity limit, $g''/2 \lesssim 4\pi$. The unitarity limits were studied in [15] and depend on the mass of the new vector triplet resonance. If we require that the top-BESS model unitarity holds up to

² Assuming that the values of G_F , $e(M_Z)$, and M_Z are fixed by measurement, the explicit formula for $g''(x)$ is given by the Eqs. (B29) and (B30).

the same energy as for the Higgsless SM — 1.7 TeV — the g'' parameter is restricted only from below: $g'' \geq 3$, 6, and 9, when $M_V = 1.0$, 1.7, and 2.3 TeV, respectively. The perturbativity limit reads $g'' \lesssim 30$.

The Eqs. (64) and (65), along with the expressions for $\epsilon_i^{\text{SM}(1)}$ and $\epsilon_i^{\kappa(1)}$ imply that ϵ_3 is the most sensitive epsilon with respect to x . Hence, our first estimation of the limit on x comes from ϵ_3 alone.

The LE-tBESS prediction of ϵ_3 can be approximated by

$$\epsilon_3 = x^2 + \epsilon_3^{\text{SM}(1)}(M_H), \quad (78)$$

where M_H is either identified with the cut-off scale $\Lambda_{\text{LE}} = M_V$, if the original top-BESS model without a scalar resonance is considered, or it is a mass of the scalar resonance added to the top-BESS model. We have compared (78) with ϵ_3^{exp} for four different values of M_H : 125 GeV, 300 GeV, 1 TeV, and 2 TeV. While the first value suits the top-BESS model with the scalar resonance imitating the recently discovered 125-GeV boson, the other three values can represent the top-BESS model without a scalar resonance.

In all these cases, $\epsilon_3^{\text{SM}(1)}(M_H)$ is larger than ϵ_3^{exp} . Thus, the Eq. (78) has no real solution for x . Nevertheless, the positive values of the difference are statistically admissible if we assume its normal distribution with the standard deviation taken from ϵ_3^{exp} . Then, the probability that the difference is positive amounts to 47%, 28%, 10%, and 5% when $M_H = 0.125$, 0.3, 1, and 2 TeV, respectively. At the same time, these numbers indicate the data support for g'' taking on any real value. The likelihood that the g'' value lies anywhere below a given value g_0'' is depicted in Fig. 1. We can see that adding the 125-GeV scalar field to the top-BESS Lagrangian improves the data support for the model.

Generally speaking, this simplified single-observable analysis provides not very convincing statistical support of the BESS-like extensions of the SM. Nevertheless, two comments seem to be in order. First, the negativity of $\epsilon_3^{\text{exp}} - \epsilon_3^{\text{SM}(1)}$ could be compensated for by adding new independent direct interactions of the vector triplet with the light fermions. It would work in the same way as the b parameter does in the BESS model [14]. Secondly, as it will be shown below, the multi-observable fitting modifies the ϵ_3 -based conclusions.

Let us turn our attention to the multi-observable fitting. More observables not only bring additional experimental input but they also make the analysis sensitive to the other-than- x free parameters. The results of the multi-observable fits are shown in Tables II and III. When fitting the Set-A, we search for the values of three LE-tBESS free parameters, x , ΔL , ΔR , that would best fit the observables $\epsilon_{1,2,3,b}$, and $\text{BR}(B \rightarrow X_s \gamma)$. When fitting the Set-B we calculate the best fits of four LE-tBESS parameters, x , ΔL , ΔR , p , to the observables $\epsilon_{1,2,3}$, Γ_b , and $\text{BR}(B \rightarrow X_s \gamma)$. Recall that, because of ϵ_b , fitting of the Set-A is applicable only when $p = 0$. There is a one-to-

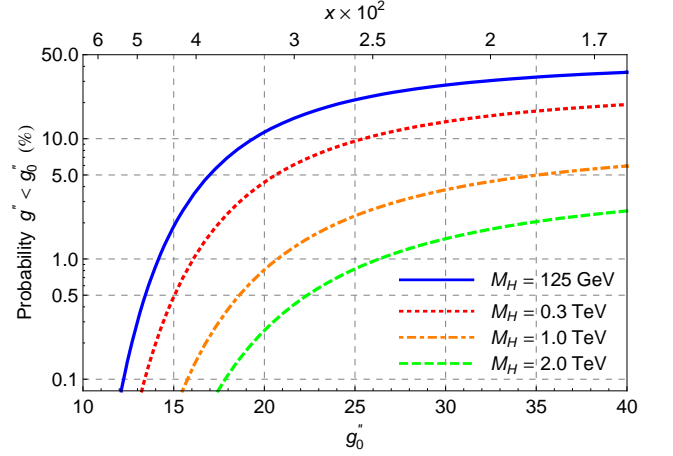


FIG. 1. (color online) The probability that g'' lies anywhere below a given value of g_0'' . It is based on ϵ_3 parameter and depends on M_H used for calculation of $\epsilon_3^{\text{SM}(1)}$. Plots for $M_H = 125$ GeV (blue solid), 0.3 TeV (red dotted), 1 TeV (orange dot-dashed), and 2 TeV (green dashed) are shown. Recall that $x = g/g''$.

TABLE II. The best-fitting values of the free parameters $\{g''(x), \Delta L, \Delta R\}$ (Set-A) and $\{g''(x), \Delta L, \Delta R, p\}$ (Set-B) obtained by fitting five observables at various fixed values of Λ that correspond to the Higgsless top-BESS model ($M_H = \Lambda$). The χ_{\min}^2 and the corresponding statistical backing of the optimized values are also shown.

Set-A (d.o.f. = 2)						
Λ (TeV)	$g''(x)$	ΔL	ΔR		χ^2_{min}	Backing (%)
0.3	77	-0.003	0.092		6.14	4.6
1	∞	-0.003	0.052		7.06	2.9
2	∞	-0.003	0.048		8.03	1.8
Set-B (d.o.f. = 1)						
Λ (TeV)	$g''(x)$	ΔL	ΔR	p	χ^2_{min}	Backing (%)
0.3	75	-0.004	0.092	0.036	2.78	9.5
1	∞	-0.006	0.052	0.063	3.70	5.4
2	∞	-0.007	0.048	0.069	4.67	3.1

TABLE III. The same as in Table II except that the 125-GeV scalar is added to the top-BESS model ($M_H = 125$ GeV).

Set-A (d.o.f. = 2)						
Λ (TeV)	$g''(x)$	ΔL	ΔR		χ^2_{min}	Backing (%)
1	29	-0.003	0.016		5.78	5.6
2	29	-0.003	0.011		5.78	5.6
Set-B (d.o.f. = 1)						
Λ (TeV)	$g''(x)$	ΔL	ΔR	p	χ^2_{min}	Backing (%)
1	29	-0.004	0.016	0.209	2.40	12.1
2	29	-0.004	0.011	0.289	2.40	12.1

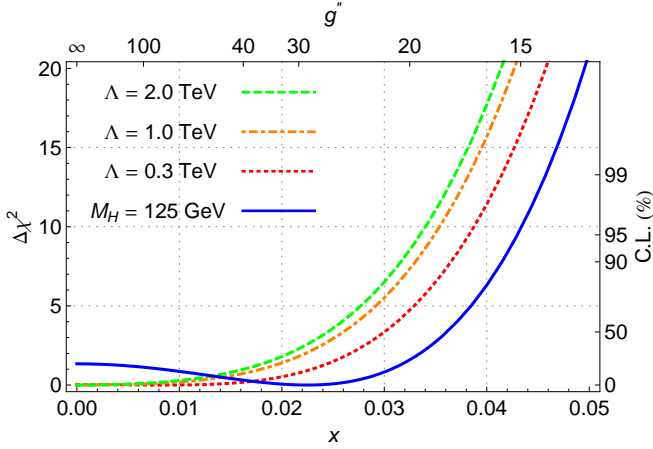


FIG. 2. (color online) $\Delta\chi^2$ as a function of x when ΔL , ΔR , and p are fixed at their optimized values found in the Set-B fit (see Tables II and III). The blue solid curve corresponds to the top-BESS model with the 125-GeV scalar boson and $\Lambda = 1$ TeV. The red dotted, orange dot-dashed, and green dashed curves correspond to the Higgsless top-BESS model with $\Lambda = 0.3, 1$, and 2 TeV, respectively. The right-hand side y -axis depicts the values of the four-dimensional confidence level limits that correspond to the $\Delta\chi^2$ labeled on the left-hand side y -axis.

one relationship between x and g'' ; in Tables II and III we list the optimized values of g'' , rather than x .

Table II corresponds to the case of the Higgsless top-BESS model. There, M_H can be considered an adjusting parameter of the used approximation. Its value is set to Λ . The best-fit values of g'' obtained for this case are very high with quite a low statistical support. In this sense, the results get worse as the value of $\Lambda = M_V$ is raised. For the Set-B, the preferred value of p is pushed close to zero. Thus, the results of the Set-A fit and the Set-B fit are almost identical.

Table III shows the optimized values of the LE-tBESS parameters with the 125-GeV resonance added. When compared with the values of Table II we observe a significant decrease of the best value of g'' . At the same time, its backing has improved. The multi-observable analysis confirms the trend deduced from the fit of ϵ_3 alone: the presence of the 125-GeV scalar boson in the top-BESS model moves g'' to lower values. The optimized value of p ranges within $0.2 - 0.3$. Thus, data prefers the right bottom-quark coupling to the vector resonance triplet to be less than 10% of the corresponding right top-quark coupling. This finding is in a general agreement with the expectations of some partial compositeness hypotheses that the degree of compositeness of the top quark is higher than it is for the bottom quark [19].

In Fig. 2 we show how $\Delta\chi^2 = \chi^2(x, \Delta L, \Delta R, p; \Lambda, M_H) - \chi^2_{min}$ depends on x (and thus on g'') when ΔL , ΔR , and p are kept at their optimized values found in the Set-B fit (see Tables II and III). On the right-hand side y -axis the confidence level values for the four-dimensional parameter space

TABLE IV. The best-fit values of the $\{\Delta L, \Delta R, p\}$ parameters in the Set-B fits of the Higgsless case ($M_H = \Lambda$) for various values of g'' and Λ . The corresponding values of χ^2_{min} and of statistical backing for d.o.f = $5 - 3 = 2$ are also shown.

Set-B (d.o.f = 2)						
Λ (TeV)	g''	ΔL	ΔR	p	χ^2_{min}	Backing (%)
0.3	10	-0.006	0.290	0.011	26.1	0.0
0.3	20	-0.005	0.135	0.024	4.1	13.1
0.3	30	-0.005	0.109	0.030	3.0	22.4
1	10	-0.008	0.111	0.030	33.8	0.0
1	20	-0.007	0.067	0.049	6.7	3.6
1	30	-0.006	0.059	0.056	4.6	9.8
2	10	-0.009	0.090	0.037	38.6	0.0
2	20	-0.007	0.058	0.057	8.6	1.4
2	30	-0.007	0.052	0.063	6.0	4.9

are labeled. Thus, for a chosen probability, we can read off the confidence level interval for x (or g'') in the $(\Delta L, \Delta R, p)$ -optimized slice of the four-dimensional parameter space. There are three curves corresponding to the Higgsless case ($\Lambda = 0.3, 1$, and 2 TeV) and the curve of the 125-GeV scalar case. While in the former there is a clear preference of very large (infinite) g'' , the latter prefers g'' of about 30. The 125-GeV scalar curve depicted in Fig. 2 has been calculated at $\Lambda = 1$ TeV. The curve is barely distinguishable from the $\Lambda = 2$ TeV case; hence, we do not show it.

B. Fitting of sub-models

In this Subsection we analyze and compare the fits of the observables when the values of some of the free parameters are fixed. Recall that if the Set-A is fitted by the LE-tBESS Lagrangian there are three fitting parameters, $\{x, \Delta L, \Delta R\}$. In the case of fitting the Set-B, there are four fitting parameters, $\{x, \Delta L, \Delta R, p\}$. However, some beyond the SM theories can result in the top-BESS effective description where one or more of these parameters are given.

We saw that in the case of the Higgsless top-BESS model the experiment pushes the value of g'' to infinity which would effectively remove the vector resonance from the game. In spite of this preference, we have performed fits when the values of g'' are fixed at 10, 20, and 30, and the cut-off scale Λ runs over 0.3, 1, and 2 TeV. The obtained best-fit values of the parameters $\{\Delta L, \Delta R, p\}$ and their backings are shown in Table IV. As we can see, for the fixed values of g'' the backing improves when the cut-off scale decreases. Unfortunately, it also implies lowering the value of the vector resonance mass which can conflict with the exclusion lower bounds obtained by the LHC.

We also saw that the inclusion of the 125-GeV scalar

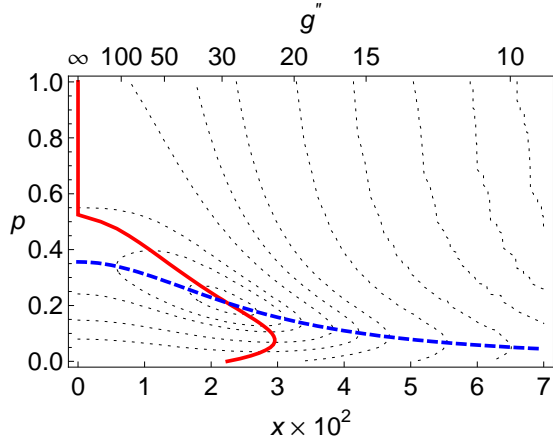


FIG. 3. (color online) The graph depicts the results of various Set-B fits when $M_H = 125$ GeV and $\Lambda = 1$ TeV. The blue dashed line shows the best-fitting value of p as a function of x with $\{\Delta L, \Delta R, p\}$ as fitting parameters. The red solid line is the best-fitting value of x as a function of p with $\{\Delta L, \Delta R, x\}$ as fitting parameters. The gray dotted contours join the (x, p) points for which the Set-B fit with $\{\Delta L, \Delta R\}$ as fitting parameters provides the same backing.

resonance into the top-BESS model has created much better situation: $g'' \approx 30$ rather than the infinity is preferred by the data. Now, let us perform the fit when either x or p are fixed. In the former case, the fitting parameters are $\{\Delta L, \Delta R, p\}$. The dashed line in Fig. 3 shows how the best-fit value of p depends on the fixed x . We can see that the preferred value of p ranges between 0 and 0.4. Thus, the vector resonance interaction with the right bottom quark weaker than with the right top quark is supported by the data. In the same graph, the solid line depicts how the best-fit value of x depends on the fixed p when the fitting parameters are $\{\Delta L, \Delta R, x\}$. The preferred values of g'' do not fall below 20.

In Fig. 3, there are also the gray dotted contours which join the (x, p) points with the same backing in the fit with $\{\Delta L, \Delta R\}$ as fitting parameters. As expected, the (x, p) point with the greatest backing in this fit corresponds to the intersection of the dashed and solid lines.

In Table V, we show the best-fit values of the parameters $\{\Delta L, \Delta R, p\}$ and the corresponding backings for the 125-GeV scalar case. The values of g'' are fixed at 10, 20, and 30 and the cut-off scale Λ is either 1 TeV or 2 TeV. The best data support at the level of 30% (d.o.f. = 2) is obtained when $g'' = 30$. Note that there is a difference between the 1 TeV and 2 TeV cases only in the best-fit values of ΔR and p .

The only observables that depend on ΔR and p are $\Gamma(B \rightarrow X_s \gamma)$ and Γ_b , while ϵ_1 depends solely on ΔR . In particular, $\Gamma(B \rightarrow X_s \gamma)$ depends on the product $p \Delta R$ while Γ_b depends on $p^2 \Delta R$. The sensitivity to Λ enters through ϵ_1 only. Scrutinizing Tables IV and V one can find that the values of the product $p \Delta R$ differ only slightly through all lines: $3.19 \leq p \Delta R \times 10^3 \leq 3.33$ (Table IV) and $3.28 \leq p \Delta R \times 10^3 \leq 3.37$ (Table V). Thus,

TABLE V. The same as in Table IV except that the 125-GeV scalar case ($M_H = 125$ GeV) is considered here.

Λ (TeV)	g''	Set-B (d.o.f = 2)				
		ΔL	ΔR	p	χ^2_{min}	Backing (%)
1	10	-0.005	0.065	0.051	21.2	0.0
1	20	-0.004	0.023	0.144	2.8	24.5
1	30	-0.004	0.015	0.215	2.4	30.1
2	10	-0.005	0.047	0.070	21.2	0.0
2	20	-0.004	0.017	0.198	2.8	24.5
2	30	-0.004	0.011	0.298	2.4	30.1

it seems that ϵ_1 and $\Gamma(B \rightarrow X_s \gamma)$ dominate the determination of the best-fit values of ΔR and p .

Figs. 4 and 5 illustrate how χ^2_{min} depends on g'' and p in the two-parameter fits of the Set-B when the fitting parameters are $\{\Delta L, \Delta R\}$. In both Figures, the right-hand y axis labels indicate the backings for d.o.f. = 5 – 2 = 3.

In Fig. 4, we show χ^2_{min} as a function of g'' for both top-BESS models, the Higgsless one as well as the 125-GeV scalar one. The former with various values of the cut-off scale Λ and the latter with $\Lambda = 1$ TeV. While the top panel contain curves when the direct vector resonance interaction to the right bottom quark is turned off, $p = 0$, in the bottom panel the p values are fixed close to the best-fit values found in the three-parameter $\{\Delta L, \Delta R, p\}$ fit (see Tables IV and V). In Fig. 5, there are the χ^2_{min} curves as function of p for the 125-GeV scalar top-BESS model with $\Lambda = 1$ TeV only. Again, we can see that the inclusion of the 125-GeV scalar into the top-BESS model improves the model's agreement with the low-energy precision data. The best-fit values of $\{\Delta L, \Delta R\}$ and the corresponding backings when d.o.f. = 3 for selected values of the given parameters g'' and p are shown in Tables VI and VII.

Using Tables VI and VII along with Tables II and III we can see the level of consistency between the fits based on the Set-A and Set-B observables. We attribute the small discrepancies to not including the $(g_{V,A}^b)^{\kappa(1)}$ contributions when calculating Γ_b of the Set-B observables as it was mentioned at the end of Subsection III B.

In Figs. 6 and 7, there are the contour maps of backings based on the Set-B $\{\Delta L, \Delta R\}$ fits of the Higgsless top-BESS model and the 125-GeV scalar top-BESS model, respectively. In this case, the best-fit values of $\{\Delta L, \Delta R\}$ and their backing depends on the given x and p . Figs. 6 and 7 depict contours of constant backing in the (x, p) parametric space. At the same time, the graphs contain the grid lines of constant best-fit values of ΔL and ΔR : $\Delta L(x, p) = \text{const}$ and $\Delta R(x, p) = \text{const}$. The grid can be used to read off the best-fit values of ΔL and ΔR for a given pair of x and p .

In Fig. 6, there are three Higgsless graphs corresponding to $\Lambda = 0.3, 1$, and 2 TeV. We can see how the low-energy precision data push g'' to infinity and p close to

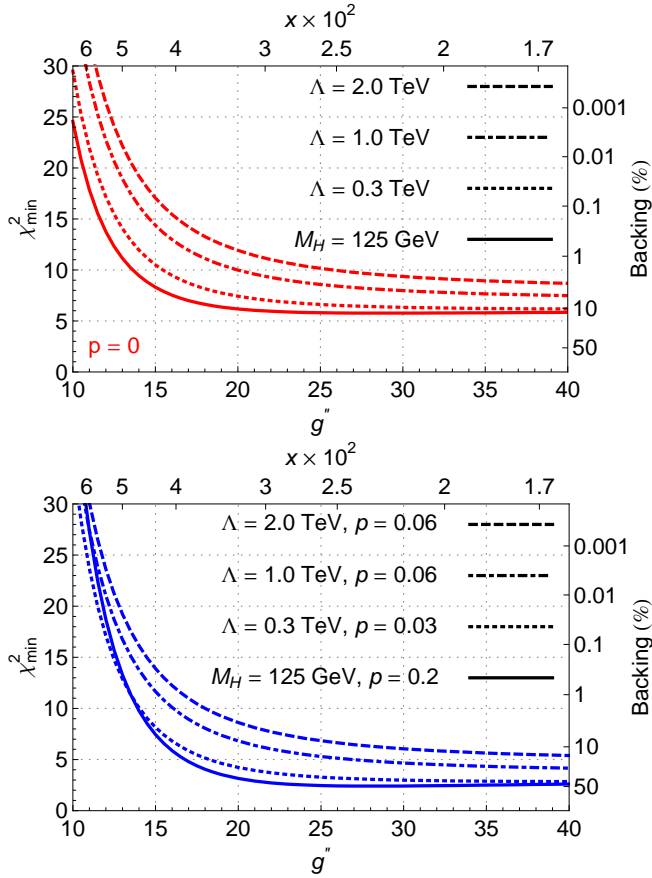


FIG. 4. (color online) χ^2_{min} of the Set-B fit as a function of g'' with $\{\Delta L, \Delta R\}$ as fitting parameters (d.o.f. = 3). The solid line corresponds to the 125-GeV scalar case with $M_H = 125$ GeV and $\Lambda = 1$ TeV. The dotted, dot-dashed, and dashed lines correspond to the Higgsless cases of $M_H = \Lambda = 0.3, 1,$ and 2 TeV, respectively. The top panel corresponds to $p = 0$. In the bottom panel, the p values are shown in the graph's legend. The right-hand y axis labels indicate the backing for d.o.f. = 3. Some of the best-fit values of ΔL and ΔR can be found in Tables VI and VII.

zero. Regarding g'' , the situation gets worse as Λ grows.

Fig. 7 shows two 125-GeV scalar graphs, one for $\Lambda = 1$ TeV, the other for $\Lambda = 2$ TeV. When compared with the Higgsless case, the preferred value of g'' moved to about 30 and the data support has risen. The preferred value of p differs from zero. Nevertheless, it still clearly suggests that the vector resonance interaction to the right bottom quark should be weaker than to the right top quark.

C. Low-energy limits in the $(\Delta L, \Delta R)$ space in the 125-GeV scalar case

For the case of the 125-GeV scalar top-BESS model we have calculated allowed regions in the $(\Delta L, \Delta R)$ parameter space based on the two-parameter fits of the Set-B observables (d.o.f. = 3). Of course, the fitting param-

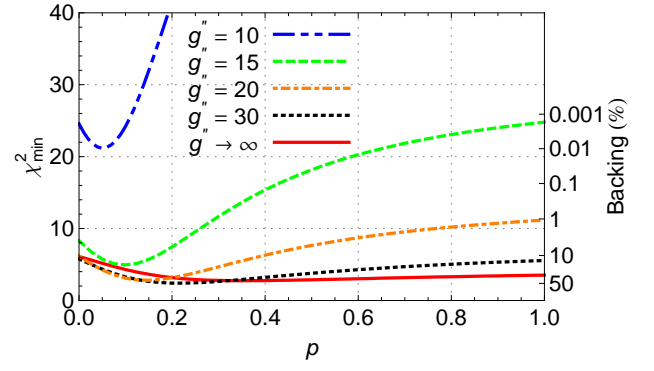


FIG. 5. (color online) χ^2_{min} of the Set-B fit as a function of p with $\{\Delta L, \Delta R\}$ as fitting parameters (d.o.f. = 3). The 125-GeV scalar case with $M_H = 125$ GeV and $\Lambda = 1$ TeV is considered only. The blue dot-dot-dashed, green dashed, orange dot-dashed, black dotted, and red solid curves correspond to $g'' = 10, 15, 20, 30,$ and $g'' \rightarrow \infty$, respectively. Some of the best-fit values of ΔL and ΔR can be found in Table VII.

TABLE VI. The best-fit values of the $\{\Delta L, \Delta R\}$ parameters in the Set-A and Set-B fits of the Higgsless case ($M_H = \Lambda$) for various values of g'' , p , and Λ . The corresponding values of χ^2_{min} and of statistical backing for d.o.f = 5 - 2 = 3 are also shown.

Set-A (d.o.f = 3)						
Λ (TeV)	g''		ΔL	ΔR	χ^2_{min}	Backing (%)
1	10		-0.005	0.111	37.2	0.0
1	20		-0.004	0.067	10.0	1.8
1	30		-0.003	0.059	8.0	4.6
Set-B (d.o.f = 3)						
Λ (TeV)	g''	p	ΔL	ΔR	χ^2_{min}	Backing (%)
0.3	10	0.03	-0.006	0.253	34.3	0.0
0.3	20	0.03	-0.005	0.131	4.2	23.7
0.3	30	0.03	-0.005	0.109	3.0	39.3
1	10	0	-0.008	0.111	37.1	0.0
1	10	0.06	-0.008	0.107	37.4	0.0
1	20	0	-0.007	0.067	10.0	1.9
1	20	0.06	-0.007	0.066	6.8	7.8
1	30	0	-0.006	0.059	8.0	4.7
1	30	0.06	-0.006	0.058	4.7	19.8
2	10	0.06	-0.009	0.089	40.1	0.0
2	20	0.06	-0.007	0.058	8.6	3.5
2	30	0.06	-0.007	0.052	6.1	10.9

eters are ΔL and ΔR , the values of g'' , p , and Λ are fixed.

In Fig. 8 we show the 90%, 95%, and 99% confidence level regions around the best-fit points with $g'' = 30$, $\Lambda = 1$ TeV, and $p = 0, 0.2, 0.5,$ and 1 . The backings of these parameter points are about 12%, 49%, 29%, and 14%, respectively. Since ΔL is predominantly related to a different observable (Γ_b) than ΔR and p ($\epsilon_1, \Gamma(B \rightarrow X_s \gamma)$), it is not unexpected that the changes

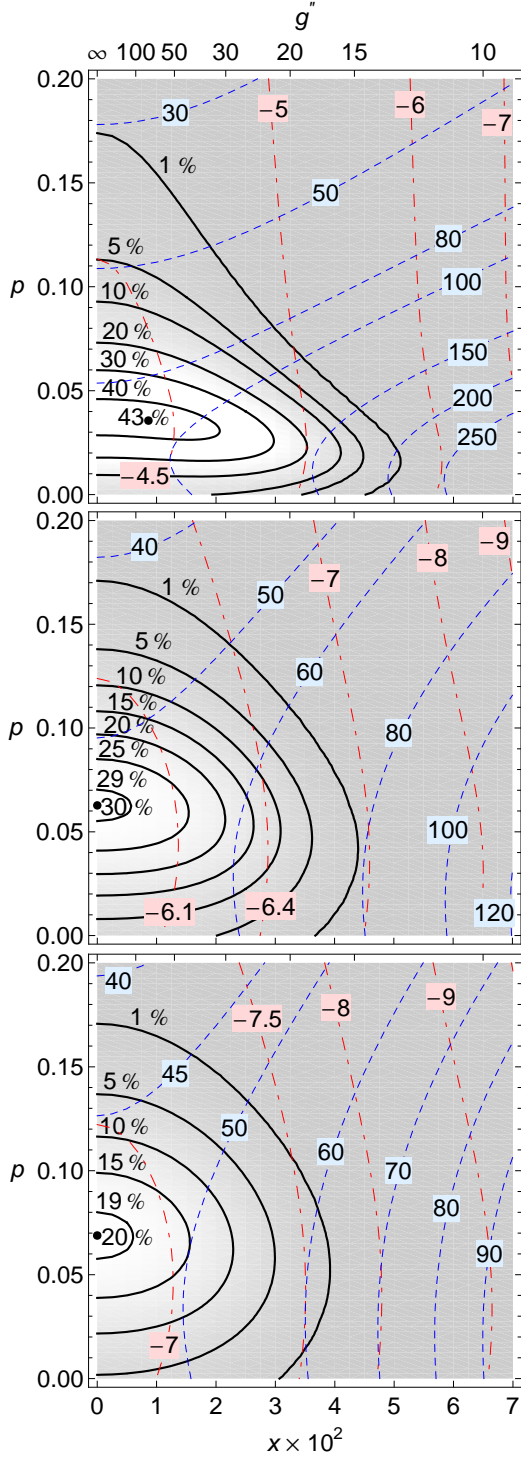


FIG. 6. (color online) The contour maps of backings as functions of x and p for the Set-B fits of the Higgsless case ($M_H = \Lambda$) with $\{\Delta L, \Delta R\}$ as fitting parameters (d.o.f. = 3). The three panels correspond to $\Lambda = 0.3, 1$, and 2 TeV, from the top to the bottom, respectively. The black solid contours connect (x, p) points of the same backing. The backing is also indicated by the shading of the background: the lighter gray means greater backing. The best-fit values of ΔL and ΔR for the given (x, p) point can be read off from the dashed-line grid. The constant values of ΔL and ΔR are represented by the red dot-dashed and blue dashed lines, respectively. The values are equal to the numbers attached to the grid lines divided by 10^3 .

TABLE VII. The same as in Table VI except that the 125-GeV scalar case ($M_H = 125$ GeV) is considered here.

Set-A (d.o.f = 3)						
Λ (TeV)	g''		ΔL	ΔR	χ^2_{min}	Backing (%)
1	10		-0.004	0.065	24.6	0.0
1	20		-0.003	0.023	6.2	10.3
1	30		-0.003	0.015	5.8	12.3
Set-B (d.o.f = 3)						
Λ (TeV)	g''	p	ΔL	ΔR	χ^2_{min}	Backing (%)
1	10	0	-0.005	0.065	24.6	0.0
1	10	0.2	-0.006	0.045	41.6	0.0
1	20	0	-0.004	0.023	6.2	10.3
1	20	0.2	-0.004	0.021	3.2	36.8
1	30	0	-0.004	0.015	5.8	12.3
1	30	0.2	-0.004	0.016	2.4	49.1
2	10	0.25	-0.006	0.035	38.4	0.0
2	30	0.25	-0.004	0.012	2.5	48.1

in p affect ΔR only. In all four displayed cases the 95% C.L. allowed interval for ΔL reads $(-0.011, 0.004)$. The 95% C.L. allowed interval for ΔR is $(-0.001, 0.032)$ when $p = 0$. It shrinks to $\Delta R \in (0.000, 0.008)$ when $p = 1$.

Fig. 9 shows the 95% C.L. allowed regions in the $(\Delta L, \Delta R)$ parameter space when p assumes the values 0.10, 0.14, 0.18, and 0.22. These are the p values with the highest backings for $g'' = 15, 20, 25$, and 30 , respectively. The corresponding backings are about 18%, 42%, 49%, and 49%. The allowed regions are shown for the cut-off scales $\Lambda = 1$ TeV and $\Lambda = 2$ TeV. As far as the allowed regions are concerned, ΔL falls within $(-0.012, 0.004)$, independently of the other parameter values. For $\Lambda = 1$ TeV, the ΔR limits read $(0.018, 0.049)$ when $g'' = 15$, $(0.009, 0.037)$ when $g'' = 20$, $(0.005, 0.032)$ when $g'' = 25$, and $(0.002, 0.028)$ when $g'' = 30$. For $\Lambda = 2$ TeV, the ΔR limits read $(0.014, 0.036)$ when $g'' = 15$, $(0.007, 0.028)$ when $g'' = 20$, $(0.004, 0.024)$ when $g'' = 25$, and $(0.002, 0.022)$ when $g'' = 30$.

D. Low-energy regions vs the Death Valley effect

In the paper [15], we had introduced and analyzed the so-called Death Valley (DV) effect. The DV is a region in the (b_L, b_R) parameter space where the interplay of the direct and indirect couplings of the vector triplet with fermions can diminish or even zero a particular top/bottom quark channel decay width of the vector resonance. Thus, it might happen that even though the direct couplings of the vector resonance to the top and/or bottom quark — proportional to $b_{L,R}$ — are non-trivial the resonance will not decay through the given quark channel. Or, the particular decay will be suppressed below the value that would be implied by the indirect cou-

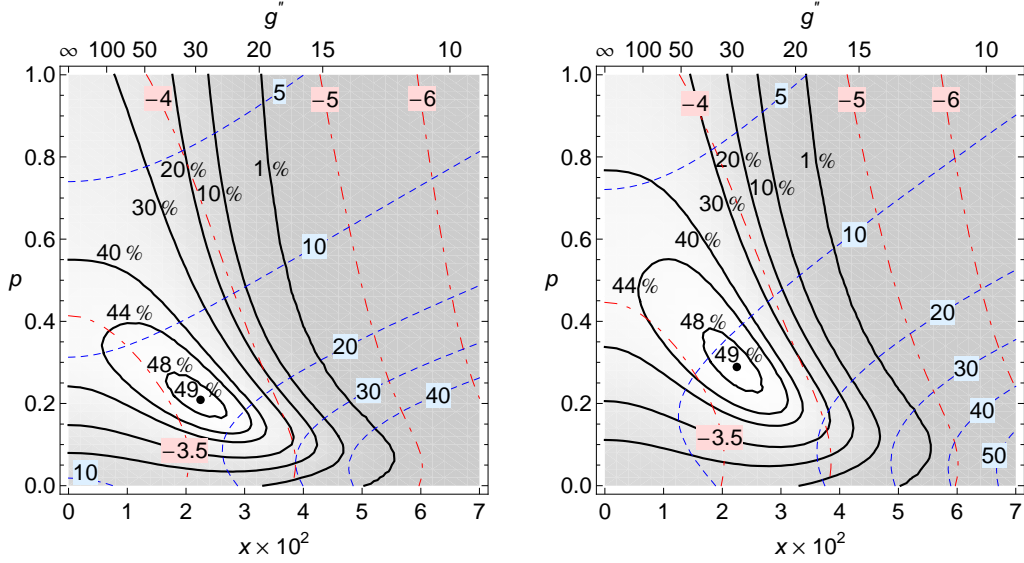


FIG. 7. (color online) The same as in Fig. 6 except that the 125-GeV scalar case ($M_H = 125$ GeV) is considered here. The left and right panels display the $\Lambda = 1$ TeV and $\Lambda = 2$ TeV cases, respectively.

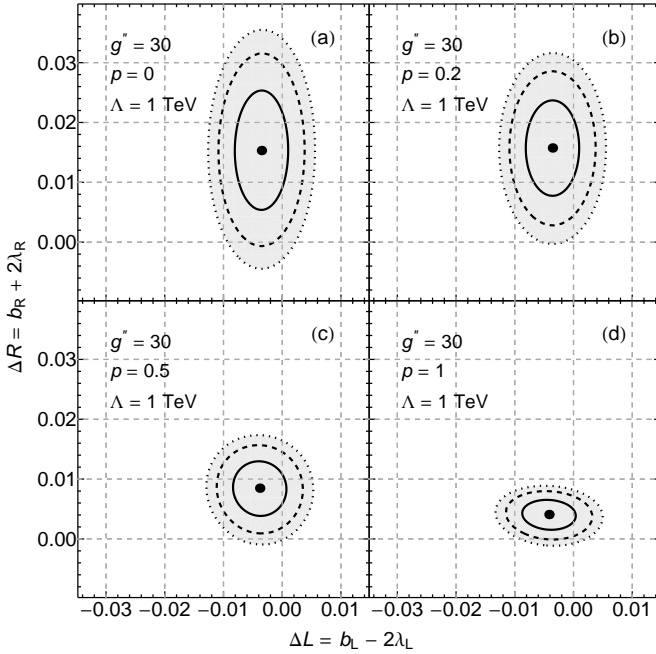


FIG. 8. 90% C.L. (solid line), 95% C.L. (dashed line), and 99% C.L. (dotted line) allowed regions in the $(\Delta L, \Delta R)$ parameter space. The regions are derived from the two-parameter fit of the Set-B observables (d.o.f. = 3) by the 125-GeV scalar top-BESS models with $g'' = 30$, $\Lambda = 1$ TeV, and $p = 0$ (a), 0.2 (b), 0.5 (c), and 1 (d). The fitting parameters are ΔL and ΔR and their best-fit values are indicated by the dots.

plings alone.

We have calculated the DV regions for $M_V = 1$ TeV and for the parameter values of Figs. 9a and 9d. That is, $(g'', p) = (15, 0.10)$ in the former case, and $(30, 0.22)$

in the latter one. For each case, the DV's in three decay channels of the vector resonance triplet have been found. The channels are $V^\pm \rightarrow t\bar{b}/\bar{t}b$, $V^0 \rightarrow b\bar{b}$, and $V^0 \rightarrow t\bar{t}$.

In Fig. 10, the DV regions of the three decay channels corresponding to Fig. 9a parameters ($g'' = 15$ and $p = 0.1$) are depicted. In each of the three graphs, there are the 95% C.L. electroweak precision data (EWPD) contours of Fig. 9a for $\Lambda = 1$ TeV superimposed. The low-energy limits apply to the combination of b 's and λ 's (ΔL and ΔR) rather than to the parameters alone. The low-energy limits depicted in the $b_R - b_L$ graphs correspond to $\lambda_L = \lambda_R = 0$. Nevertheless, by choosing non-zero values for $\lambda_{L,R}$ the low-energy contours get shifted around the (b_L, b_R) parameter space. Various values of λ 's can result either in no overlap of the low-energy regions with the DV's or in maximal overlap of the two areas.

Fig. 11 displays the same contents as Fig. 10, except for different values of the parameters g'' and p . Here, the values of the parameters correspond to Fig. 9d: $g'' = 30$ and $p = 0.22$. There are also the 95% C.L. electroweak precision data contours of Fig. 9d for $\Lambda = 1$ TeV and $\lambda_L = \lambda_R = 0$ superimposed in Fig. 11.

As we can see in Figs. 10 and 11 the DV areas are more or less comparable in size with the EWPD regions. In addition, both structures are located not far away from each other when $\lambda_L = \lambda_R = 0$. Hence, there are reasonable values of the λ parameters for which the significant part of an EPWD region falls inside the DV.

There might be new physics materialized through the existence of the new vector resonances as well as non-zero values of the b parameters, yet it does not have to reveal itself in an experiment. If the actual values of the b parameters fell in the DV it would make the detection and study of the new vector resonance more difficult. In par-

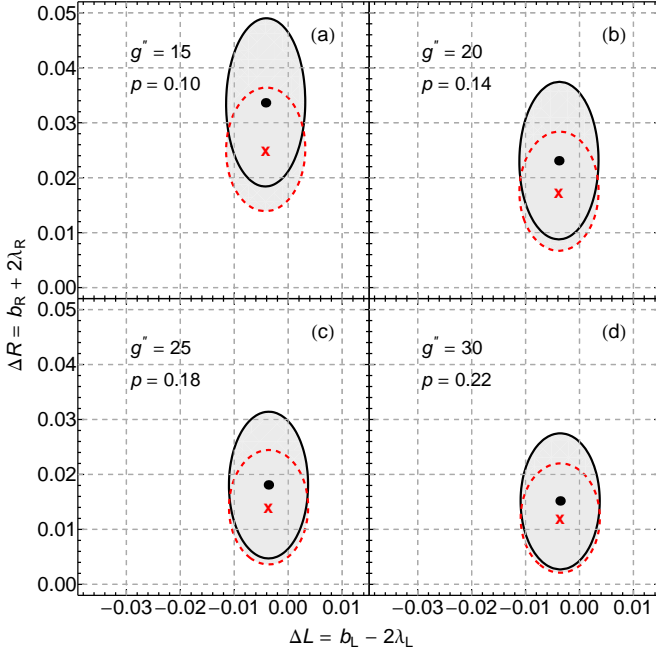


FIG. 9. (color online) 95% C.L. allowed regions in the $(\Delta L, \Delta R)$ parameter space derived from the same fit as in Fig. 8 except for the values of the fixed parameters. The black solid contours correspond to $\Lambda = 1$ TeV, the red dashed ones to $\Lambda = 2$ TeV. The values of the fixed parameters g'' and p are, respectively, 15 and 0.10 (a), 20 and 0.14 (b), 25 and 0.18 (c), 30 and 0.22 (d). The best-fit values of ΔL and ΔR are indicated by the black dot and red cross for $\Lambda = 1$ TeV and $\Lambda = 2$ TeV, respectively.

ticular, thanks to the indirect mixing-induced coupling the vector resonance can be produced and studied in the Drell-Yan processes at the LHC or in the s-channel at a future electron-positron collider [30, 31]. As we demonstrated in [15] the signal of the vector resonance in the top and bottom decay channels can be diminished or hidden by the negative interference between the direct and indirect couplings.

V. CONCLUSIONS

The top-BESS effective Lagrangian describing the phenomenology of the $SU(2)$ vector resonance triplet was extended to study the impact of a newly discovered 125-GeV boson on the low-energy limits and the statistical support for the model. We opted for the assumption that the boson was a scalar with the SM-like parameters. The χ^2 analysis based on the epsilon pseudo-observables, $\Gamma_b(Z \rightarrow b\bar{b} + X)$, and $\text{BR}(B \rightarrow X_s \gamma)$, resulted in finding the best-fit values and the backings for the vector resonance gauge coupling g'' and for three parameters responsible for the direct vector resonance couplings to the top and bottom quarks, $\Delta L = b_L - 2\lambda_L$, $\Delta R = b_R + 2\lambda_R$, and p . The analysis was performed assuming TeV values of the vector resonance mass.

Without the scalar resonance the low-energy data pushed the preferred value of g'' to infinity which would effectively amount to removing the vector resonance from the model's spectrum. In addition, when $g'' \gtrsim 30$ we enter the non-perturbative regime in which our conclusions are questionable. The optimal value of p was approaching zero which would amount to turning off the vector resonance coupling to the right bottom quark. The maximum data backing for this scenario did not exceed 30%.

After the scalar resonance had been added the situation improved in a couple of ways. The most preferred value of g'' decreased to about 30 and its backing grew to about 50%. The best-fit value of p ranges between 0.2 and 0.3 for $M_V = 1$ TeV and 2 TeV, respectively. This result suggests the preferred role of the top quark in physics responsible for ESB. Recall that in the top-BESS model the $V^\pm t_R b_R$ vertex is suppressed by the factor p while the suppression factor of the $V^0 b_R b_R$ vertex relative to $V^0 t_R t_R$ is p^2 .

We calculated the 95% confidence level allowed regions around the best-fit values of ΔL and ΔR when g'' and p had been fixed. This imitates the situation when the concerned parameters were constrained by theoretical assumptions. We chose $g'' = 15, 20, 25$, and 30 and $p = 0.10, 0.14, 0.18$, and 0.22, respectively. The values of p were fixed at their best-fit values for the given g'' 's. The backings for the corresponding best-fit values of $(\Delta L, \Delta R)$ were 18%, 42%, 49%, and 49%, respectively, with d.o.f. = 3. For all these settings, the 95% C.L. interval of ΔL is $(-0.012, 0.004)$. When $M_V = 1$ TeV the 95% C.L. interval of ΔR shrinks from $(0.018, 0.049)$ at $g'' = 15$ to $(0.002, 0.028)$ at $g'' = 30$. Raising M_V to 2 TeV did not affect the 95% C.L. interval for ΔL . The 95% C.L. interval for ΔR changes from $(0.014, 0.036)$ at $g'' = 15$ to $(0.002, 0.022)$ at $g'' = 30$.

There might be new physics materialized through the existence of the new vector resonances as well as non-zero values of the b parameters, yet it does not have to reveal itself in an experiment. Even though there are no direct interactions of the vector resonance triplet to the light fermions the resonance does couple to the light fermions thanks to the mixing with the electroweak gauge bosons. This enables processes with a direct production of the vector resonance at the LHC and future electron-positron colliders. However, in the top and bottom decay channels the signal of the vector resonance can be diminished or hidden by the negative interference between the direct and indirect couplings. We calculated the regions of the negative interference for the studied values of the top-BESS parameters and found that they are often comparable in size and close in position with the 95% C.L. regions. As a general tendency, the relative size of the DV's with respect to the low-energy allowed areas shrinks as the value of g'' grows.

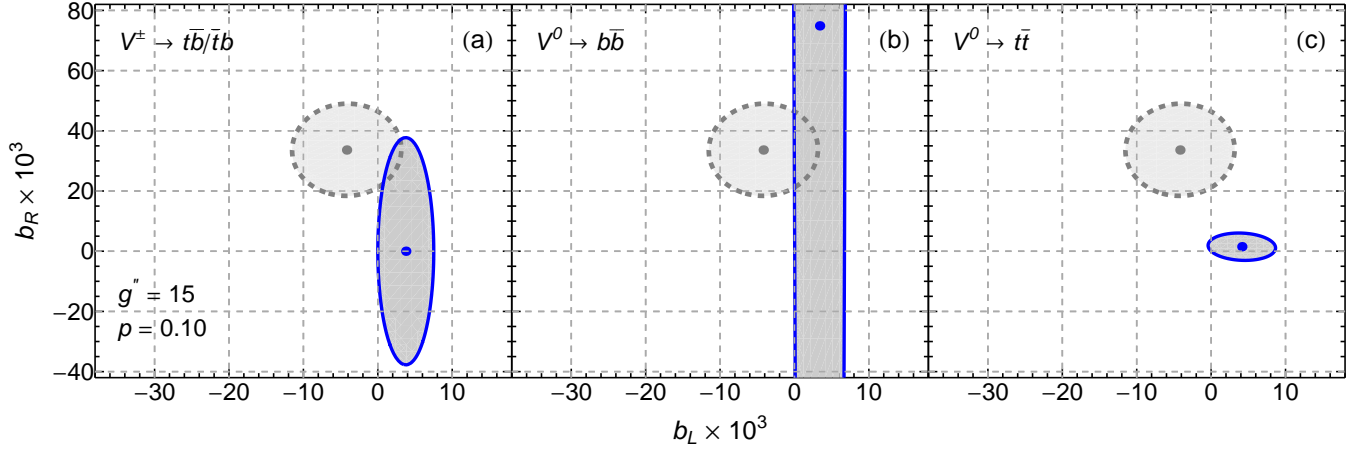


FIG. 10. (color online) The DV regions (dark-shaded areas with the blue solid boundary) of the $M_V = 1$ TeV vector resonance for three decay channels: (a) $V^\pm \rightarrow t\bar{b}/\bar{t}b$, (b) $V^0 \rightarrow b\bar{b}$, and (c) $V^0 \rightarrow t\bar{t}$. The blue dots inside the DV's indicate the point of no decay for the particular channels. The DV regions are calculated for $g'' = 15$ and $p = 0.10$. The corresponding 95% C.L. EWPD contours for $\Lambda = 1$ TeV and $\lambda_L = \lambda_R = 0$ are superimposed to the graphs as the regions with the gray dashed boundaries. The gray dots inside the EWPD regions indicate the point with the highest backing. Note that the DV for the $V^0 \rightarrow b\bar{b}$ channel exceeds the displayed range of the b_R axis. The complete DV region has an oval shape centered at the blue dot. Its lower and upper ends are found at $b_R = -0.272$ and $b_R = 0.422$, respectively.

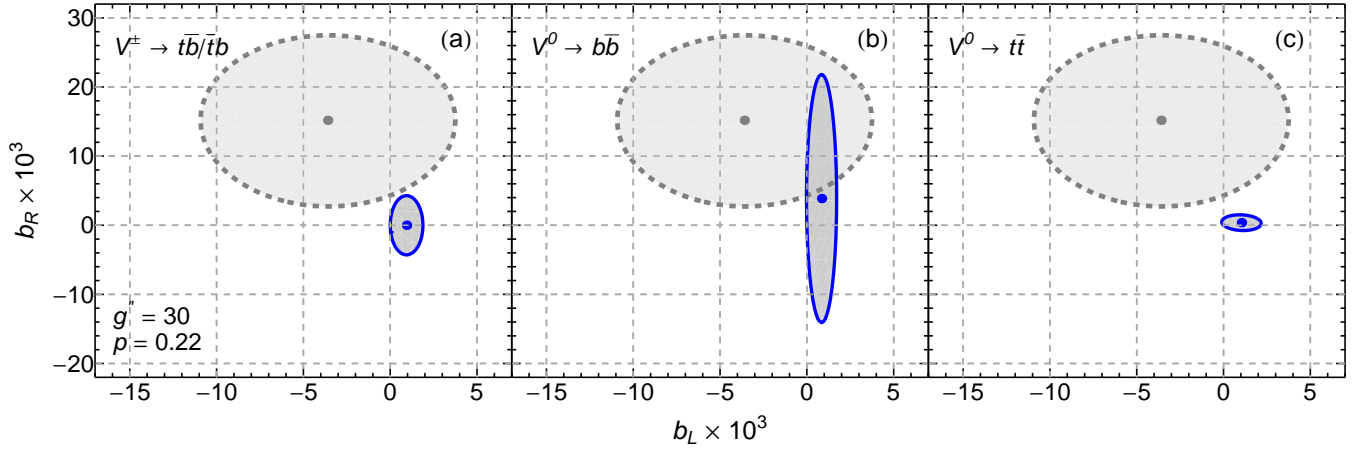


FIG. 11. (color online) The same as in Fig. 10 except for different values of g'' and p . In this case, $g'' = 30$ and $p = 0.22$.

ACKNOWLEDGMENTS

We would like to thank Ivan Melo for useful discussions. The work of M.G. and J.J. was supported by the Research Program MSM6840770029 and by the project International Cooperation ATLAS-CERN of the Ministry of Education, Youth and Sports of the Czech Republic. M.G. was supported by the Slovak CERN Fund. J.J. was supported by the NSP grant of the Slovak Republic. We would also like to thank the Slovak Institute for Basic Research for their support.

Appendix A: Experimental values

In our analyses we have used the experimental values of the epsilon pseudo-observables obtained from a fit to all LEP-I and SLD measurements including the combined preliminary measurement of the W -boson mass [32]

$$\epsilon_1^{\text{exp}} = (+5.4 \pm 1.0) \times 10^{-3}, \quad (\text{A1})$$

$$\epsilon_2^{\text{exp}} = (-8.9 \pm 1.2) \times 10^{-3}, \quad (\text{A2})$$

$$\epsilon_3^{\text{exp}} = (+5.34 \pm 0.94) \times 10^{-3}, \quad (\text{A3})$$

$$\epsilon_b^{\text{exp}} = (-5.0 \pm 1.6) \times 10^{-3}, \quad (\text{A4})$$

with the correlation matrix

$$\rho^\epsilon = \begin{pmatrix} 1.00 & 0.60 & 0.86 & 0.00 \\ 0.60 & 1.00 & 0.40 & -0.01 \\ 0.86 & 0.40 & 1.00 & 0.02 \\ 0.00 & -0.01 & 0.02 & 1.00 \end{pmatrix}. \quad (\text{A5})$$

The value of the $Z \rightarrow b\bar{b}$ decay width

$$\Gamma_b^{\text{exp}} = (0.3773 \pm 0.0013) \text{ GeV} \quad (\text{A6})$$

has been obtained from the experimental values [33]

$$\text{BR}(Z \rightarrow b\bar{b})^{\text{exp}} = (0.1512 \pm 0.0005), \quad (\text{A7})$$

$$\Gamma_{\text{tot}}(Z)^{\text{exp}} = (2.4952 \pm 0.0023) \text{ GeV}. \quad (\text{A8})$$

When fitting the set $\{\epsilon_1, \epsilon_2, \epsilon_3, \Gamma_b\}^{\text{exp}}$ the correlations between Γ_b and $\epsilon_{1,2,3}$ have been neglected.

For the branching fraction of $B \rightarrow X_s \gamma$ we have used the world average [34] (CLEO, Belle, BaBar)

$$\text{BR}(B \rightarrow X_s \gamma)^{\text{exp}} = (3.55 \pm 0.26) \times 10^{-4}. \quad (\text{A9})$$

We have considered no correlations between $\text{BR}(B \rightarrow X_s \gamma)$ and any of the observables $\epsilon_1, \epsilon_2, \epsilon_3, \epsilon_b, \Gamma_b$.

Below we will complete the list of numerical values that have been used in the calculations of this paper

$$\alpha(0) = 1/137.036, \quad (\text{A10})$$

$$\alpha(M_Z^2) = 1/128.91, \quad (\text{A11})$$

$$\alpha_s(M_Z^2) = 0.1184, \quad (\text{A12})$$

$$G_F = 1.166364 \times 10^{-5} \text{ GeV}^{-2}, \quad (\text{A13})$$

$$m_b = 4.67 \text{ GeV}, \quad (\text{A14})$$

$$m_t = 172.7 \text{ GeV}, \quad (\text{A15})$$

$$M_Z = 91.1876 \text{ GeV}. \quad (\text{A16})$$

Then, using the Eq. (32) the numerical value of s_0^2 is

$$s_0^2 = 0.2311. \quad (\text{A17})$$

Appendix B: Low-energy top-BESS Lagrangian

To obtain the low-energy limits on the top-BESS parameters we have derived the low-energy Lagrangian (LE-tBESS) by integrating out the vector triplet from the top-BESS Lagrangian with the 125 GeV scalar resonance (24). It proceeds by taking the limit $M_{\text{triplet}} \rightarrow \infty$, while g'' is finite and fixed, and by substituting the equation of motion (EofM) for the triplet fields obtained under these conditions. Most of the time the obtained relations shown in this Appendix are identical with those of the top-BESS Lagrangian without the scalar resonance. We will point out any differences that will be encountered.

The EofM in the unitarity gauge reads

$$i \frac{g''}{2} V_\mu^a = \frac{1}{2} (i g W_\mu^a + i g' B_\mu \delta^{a3}), \quad (\text{B1})$$

where $a = 1, 2, 3$.

The gauge boson kinetic terms of the LE-tBESS Lagrangian in the unitary gauge read

$$\begin{aligned} \mathcal{L}_{\text{kin}}^{\text{LE}}(A', Z') &= -\frac{1}{4}(1 + z_z)F_{\mu\nu}(Z')F^{\mu\nu}(Z') \\ &\quad -\frac{1}{4}(1 + z_\gamma)F_{\mu\nu}(A')F^{\mu\nu}(A') \\ &\quad +\frac{1}{2}z_{z\gamma}F_{\mu\nu}(Z')F^{\mu\nu}(A'), \end{aligned} \quad (\text{B2})$$

$$\begin{aligned} \mathcal{L}_{\text{kin}}^{\text{LE}}(W^{\pm'}) &= -\frac{1}{4}(1 + x^2) [F_{\mu\nu}^\dagger(W^{+'})F^{\mu\nu}(W^{+'}) \\ &\quad + F_{\mu\nu}^\dagger(W^{-'})F^{\mu\nu}(W^{-'})], \end{aligned} \quad (\text{B3})$$

where $F_{\mu\nu}(X) \equiv \partial_\mu X_\nu - \partial_\nu X_\mu$, and

$$z_z = \left(\frac{c_{2\theta}}{c_\theta} x \right)^2, \quad z_\gamma = 4s_\theta^2 x^2, \quad z_{z\gamma} = -\sqrt{z_z z_\gamma}, \quad (\text{B4})$$

where

$$x \equiv \frac{g}{g''}. \quad (\text{B5})$$

The primed fields are the gauge fields of the top-BESS Lagrangian in the mass eigenstate basis and s_θ, c_θ are the elements of the transformations matrix taking (W_μ^3, B_μ) to (Z'_μ, A'_μ) .

To obtain the canonical kinetic terms for the LE-tBESS Lagrangian the fields must undergo the following set of transformation

$$Z'_\mu = \sqrt{\frac{1 + z_\gamma}{1 + z_\gamma + z_z}} Z_\mu, \quad (\text{B6})$$

$$A'_\mu = \frac{z_{z\gamma}}{\sqrt{(1 + z_\gamma)(1 + z_\gamma + z_z)}} Z_\mu + \frac{1}{\sqrt{1 + z_\gamma}} A_\mu, \quad (\text{B7})$$

$$W_\mu^{\pm'} = \frac{1}{\sqrt{1 + x^2}} W_\mu^\pm. \quad (\text{B8})$$

Then, the masses of the “low-energy” electroweak gauge fields Z_μ and W_μ^\pm are given by the expressions

$$M_Z^2 = \frac{1 + z_\gamma}{1 + z_\gamma + z_z} \frac{G^2 v^2}{4}, \quad (\text{B9})$$

$$M_W^2 = \frac{1}{1 + x^2} \frac{g^2 v^2}{4}, \quad (\text{B10})$$

where $G = \sqrt{g^2 + g'^2}$. However, it is convenient to choose x, s_θ , and M_Z as input parameters of the LE-tBESS Lagrangian. Then, the mass of the W boson is a function of these parameters

$$M_W = M_Z c_\theta \sqrt{\frac{1 + (x/c_\theta)^2}{(1 + 4s_\theta^2 x^2)(1 + x^2)}}. \quad (\text{B11})$$

Let us turn our attention to the fermion sector of the LE-tBESS Lagrangian. After integrating out the vector triplet we end up with the low-energy Lagrangian $\mathcal{L}_{\text{ferm}}^{\text{LE}}$ in the unitarity gauge expressed in terms of the top-BESS gauge fields $A'_\mu, Z'_\mu, W_\mu^{\pm'}$. Eventually, to find the form

of the low-energy fermion interactions the renormalized fields (B6) – (B8) have to be substituted in. Then³,

$$\begin{aligned}\mathcal{L}_{\text{ferm}}^{\text{LE}} = & i\bar{\psi}\not{\partial}\psi - e\bar{\psi}\not{A}Q\psi - \frac{G_N}{2}\bar{\psi}\not{Z}(C_L P_L + C_R P_R)\psi \\ & - \frac{G_C c_\theta}{\sqrt{2}}\bar{\psi}(W^+\tau^+ + W^-\tau^-)(D_L P_L + D_R P_R)\psi \\ & - (\bar{\psi}_L M_f \psi_R + \text{H.c.})(1 + h/v),\end{aligned}\quad (\text{B12})$$

where ψ are fermion $SU(2)$ doublets, $\tau^\pm = \tau^1 \pm i\tau^2$, $P_{L,R} = (1 \mp \gamma_5)/2$, $M_f = \text{diag}(m_u, m_d)$ is a fermion mass matrix⁴, and

$$G_N = \frac{e}{s_\theta c_\theta} \frac{1 + z_\gamma}{\sqrt{1 + z_\gamma + z_z}}, \quad G_C = \frac{e}{s_\theta c_\theta} \sqrt{\frac{1 + z_\gamma}{1 + x^2}}. \quad (\text{B13})$$

For the light fermions (all SM fermions except the top and bottom quarks)

$$C_L = 2(T_L^3 - s_\theta^2 Q) - 2s_\theta c_\theta \frac{\sqrt{z_\gamma z_z}}{1 + z_\gamma} Q_f, \quad (\text{B14})$$

$$C_R = -2s_\theta^2 Q - 2s_\theta c_\theta \frac{\sqrt{z_\gamma z_z}}{1 + z_\gamma} Q_f, \quad (\text{B15})$$

and $D_L = 1$, $D_R = 0$. In the case of the top and bottom quarks

$$C_L = 2[(1 - \Delta L/2)T_L^3 - s_\theta^2 Q] - 2s_\theta c_\theta \frac{\sqrt{z_\gamma z_z}}{1 + z_\gamma} Q_f, \quad (\text{B16})$$

$$C_R = 2(P_f \Delta R T_R^3/2 - s_\theta^2 Q) - 2s_\theta c_\theta \frac{\sqrt{z_\gamma z_z}}{1 + z_\gamma} Q_f, \quad (\text{B17})$$

where $P_t = 1$, $P_b = p^2$, and

$$D_L = 1 - \Delta L/2, \quad D_R = p \Delta R/2. \quad (\text{B18})$$

The following list contains a convenient choice of independent input parameters for the LE-tBESS Lagrangian

$$e, s_\theta, x, M_Z, \Delta L, \Delta R, p, \{m_f\}, \quad (\text{B19})$$

where $\{m_f\}$ are the non-negligible fermion masses. The list of independent input parameters of the top-BESS model, natural from the point of view of the model construction, reads

$$g, g', g'', \alpha, v, b_L, b_R, \lambda_L, \lambda_R, p, \{m_f\}. \quad (\text{B20})$$

Of course, the parameters (B19) are related to the parameters (B20) of the underlying theory. Thus, the electric charge relation to the top-BESS parameters reads

$$e = \frac{gg'g''}{\sqrt{(gg'')^2 + (g'g'')^2 + (2gg')^2}}. \quad (\text{B21})$$

Further,

$$s_\theta = \frac{g'}{\sqrt{g^2 + g'^2}}, \quad x = \frac{g}{g''}. \quad (\text{B22})$$

The Z -boson mass relation is given by

$$M_Z^2 = \frac{(gg'')^2 + (g'g'')^2 + (2gg')^2}{g^2 + g'^2 + g''^2} \frac{v^2}{4}. \quad (\text{B23})$$

Finally,

$$\Delta L = b_L - 2\lambda_L, \quad \Delta R = b_R + 2\lambda_R. \quad (\text{B24})$$

In the LE-tBESS model the Fermi coupling G_F is related to e , s_θ , M_Z , and x

$$\frac{G_F}{\sqrt{2}} = \frac{1}{2} \left(\frac{e}{2s_\theta c_\theta M_Z} \right)^2 \frac{(1 + 4s_\theta^2 x^2)^2}{1 + (\frac{x}{c_\theta})^2}. \quad (\text{B25})$$

If the values of G_F , $e(M_Z)$, and M_Z are fixed by measurements then we can obtain s_θ as a function of x : $s_\theta(x; e(M_Z), M_Z, G_F)$. However, as mentioned in Section III A, G_F can be replaced by s_0 using the SM relation (32). Comparing (B25) with (32), the following relation between s_θ and s_0 must hold

$$s_0 c_0 = s_\theta c_\theta \frac{\sqrt{1 + (\frac{x}{c_\theta})^2}}{1 + 4s_\theta^2 x^2}. \quad (\text{B26})$$

Note that using the s_0 parameter for determination of s_θ eliminates, beside G_F , also $e(M_Z)$ and M_Z ; or, in other words, for the given value of s_0 , s_θ is a function of x only, $s_\theta(x; s_0)$. The acceptable solution of the implicit equation for s_θ (B26) reads

$$s_\theta = \sqrt{\frac{1 + c_{40}x^2 - (1 + x^2)\sqrt{1 - s_{20}^2 \left(\frac{1+2x^2}{1+x^2}\right)^2}}{2(1 + 4s_{20}^2 x^4)}} \quad (\text{B27})$$

assuming $c_\theta > 0$ and defining $s_{20} \equiv 2s_0 c_0$, $c_{40} \equiv c_{20}^2 - s_{20}^2$. Further, as a consequence of (B26) the couplings G_N and G_C can be expressed in the way that will prove useful for deriving LE-tBESS contributions to the anomalous fermion couplings

$$G_N = \frac{e}{s_0 c_0}, \quad G_C c_\theta = \frac{e}{s_0} \left(\frac{s_0}{s_\theta} \sqrt{\frac{1 + z_\gamma}{1 + x^2}} \right). \quad (\text{B28})$$

Given the measured values of G_F , $e(M_Z)$, and M_Z (or, alternatively, s_0 , $\alpha(M_Z)$, and M_Z), the top-BESS parameters g and g'' depend on x in the following way

$$g(x) = \frac{e(M_Z)}{\sqrt{2}s_0 c_0} \left[1 + x^2 + \sqrt{c_{20}^2(1 + x^2)^2 - s_{20}^2 x^2(2 + 3x^2)} \right]^{1/2}, \quad (\text{B29})$$

$$g''(x) = \frac{g(x)}{x}. \quad (\text{B30})$$

³ To obtain $\mathcal{L}_{\text{ferm}}^{\text{LE}}$ for the case of the top-BESS model without the scalar resonance set the scalar field to zero, $h = 0$, in the Eq. (B12).

⁴ Therein, m_u and m_d stand for the masses of any of the upper and lower components of the fermion $SU(2)$ doublets, respectively.

The leading terms of the series expansion of g in x around $x = 0$ reads

$$g(x) = \frac{e}{s_0} \left[1 + \left(1 - \frac{1}{2c_{20}} \right) x^2 + \mathcal{O}(x^4) \right]. \quad (\text{B31})$$

We often wish to find the value of x which corresponds to a given g'' . In other words, we need a formula inverse to (B30). It reads

$$x(\eta) = \frac{\eta}{\sqrt{2}} \left(1 - \eta^2 - \sqrt{1 - \eta^2 - s_{20}^2} \right)^{-1/2}, \quad (\text{B32})$$

where

$$\eta = \frac{\sqrt{16\pi\alpha(M_Z)}}{g''} = \frac{2e(M_Z)}{g''} \approx \frac{0.624}{g''}. \quad (\text{B33})$$

The leading terms of the series expansion of $x(\eta)$ in η around $\eta = 0$ read

$$x = \frac{\eta}{2s_0} \left[1 + \frac{2c_{20} - 1}{2c_{20}} \left(\frac{\eta}{2s_0} \right)^2 + \mathcal{O}(\eta^4) \right], \quad (\text{B34})$$

where $\eta/(2s_0) = e(M_Z)/(s_0 g'')$.

Appendix C: The χ^2 -test

In this Appendix we summarize the relations used in the paper for statistical calculations concerning the χ^2 -test.

First of all, the χ^2 -function is defined as

$$\chi^2 = \sum_{i=1}^n \sum_{j=1}^n (O_i - O_i^{exp}) [(\sigma^2)^{-1}]_{ij} (O_j - O_j^{exp}), \quad (\text{C1})$$

where O_j^{exp} is the measured value of an observable, O_j is its value predicted by theory, and σ^2 is the covariance matrix

$$(\sigma^2)_{ij} = \sigma_i \rho_{ij} \sigma_j, \quad (\text{C2})$$

σ_i is the standard deviation of an observable O_i , and ρ_{ij} is the correlation matrix.

Usually, the theoretical prediction depends on several free parameters p_i , $O_j(p_1, \dots, p_k)$. The best fit of the given theory to the given set of measured observables $\{O_1^{exp}, \dots, O_n^{exp}\}$ is provided by such values of $\{p_1, \dots, p_k\}$ that minimize the function χ^2 .

The statistical support for the best-fit values of the fitting parameters is given by the *backing*

$$\text{Backing} = \int_{\chi_{min}^2}^{\infty} f(z; \text{d.o.f.}) dz, \quad (\text{C3})$$

where $f(z; \text{d.o.f.})$ is the probability density distribution of χ^2 for d.o.f. = $n - k$, and χ_{min}^2 is the global minimum of χ^2 .

TABLE VIII. The values of $\Delta\chi^2$ for selected C.L. when $k = 1, 2, 3$, and 4.

k	1	2	3	4
C.L. (%)	$\Delta\chi^2$			
90	2.71	4.61	6.25	7.78
95	3.84	5.99	7.81	9.49
99	6.63	9.21	11.34	13.28

The probability — the confidence level — that the true values of the free parameters lie within the region of the (p_1, \dots, p_k) parameter space for which

$$\chi^2(p_1, \dots, p_k) - \chi_{min}^2 \leq \Delta\chi^2 \quad (\text{C4})$$

is equal to

$$\text{C.L.} = \int_0^{\Delta\chi^2} f(z; k) dz = 1 - \int_{\Delta\chi^2}^{\infty} f(z; k) dz. \quad (\text{C5})$$

For the reader's convenience we provide Table VIII relating some values of C.L. and $\Delta\chi^2$ for $k = 1, 2, 3$, and 4.

-
- [1] G. Aad *et al.* (ATLAS Collaboration), Phys. Lett. B **716**, 1 (2012); S. Chatrchyan *et al.* (CMS Collaboration), *ibid.* **30** (2012).
- [2] J. Ellis and T. You, J. High Energy Phys. **09** (2012) 123.
- [3] P. P. Giardino, K. Kannike, M. Raidal, and A. Strumia, Phys. Lett. B **718**, 469 (2012); D. Carmi, A. Falkowski, E. Kuflik, T. Volansky, and J. Zupan, J. High Energy Phys. **10** (2012) 196; M. Montull and F. Riva, *ibid.* **11** (2012) 018; T. Plehn and M. Rauch, Europhys. Lett. **100**, 11002 (2012).
- [4] M. E. Peskin, [arXiv:1208.5152](https://arxiv.org/abs/1208.5152).
- [5] S. Weinberg, Phys. Rev. D **19**, 1277 (1979); L. Susskind, *ibid.* **20**, 2619 (1979); E. Farhi and L. Susskind, Phys. Rept. **74**, 277 (1981).
- [6] S. Dimopoulos and L. Susskind, Nucl. Phys. **B155**, 237 (1979); E. Eichten and K. D. Lane, Phys. Lett. **B90**, 125 (1980).
- [7] B. Holdom, Phys. Rev. D **24**, 1441 (1981); Phys. Lett. **B150**, 301 (1985); K. Yamawaki, M. Bando, and K.-i. Matumoto, Phys. Rev. Lett. **56**, 1335 (1986); T. Appelquist, D. Karabali, and L. C. R. Wijewardhana, *ibid.* **57**, 957 (1986); T. Akiba and T. Yanagida, Phys. Lett. **B169**, 432 (1986); T. Appelquist and L. C. R. Wijewardhana, Phys. Rev. D **36**, 568 (1987); K. Lane and E. Eichten, Phys. Lett. **B222**, 274 (1989).
- [8] C. T. Hill, Phys. Lett. **B266**, 419 (1991); **B345**, 483

- (1995).
- [9] S. Matsuzaki and K. Yamawaki, Phys. Rev. D **86**, 035025 (2012); Ch. D. Carone, *ibid.* **86**, 055011 (2012); P. Athron, S. F. King, D. J. Miller, S. Moretti, and R. Nevzorov, *ibid.* **86**, 095003 (2012); S. Matsuzaki and K. Yamawaki, *ibid.* **86**, 115004 (2012); M. Geller, S. Bar-Shalom, G. Eilam, and A. Soni, *ibid.* **86**, 115008 (2012); M. Hirsch, F. R. Joaquim, and A. Vicente, J. High Energy Phys. 11 (2012) 105.
 - [10] L. D. Landau, Dokl. Akad. Nauk USSR Ser. Fiz. **60**, 207 (1948); C.-N. Yang, Phys. Rev. **77**, 242 (1950).
 - [11] D. B. Kaplan, H. Georgi, and S. Dimopoulos, Phys. Lett. **136B**, 187 (1984); H. Georgi and D. B. Kaplan, *ibid.* **145B**, 216 (1984); M. J. Dugan, H. Georgi, and D. B. Kaplan, Nucl. Phys. **B254**, 299 (1985).
 - [12] N. Arkani-Hamed, S. Dimopoulos, and G. Dvali, Phys. Lett. **B429**, 263 (1998); I. Antoniadis, N. Arkani-Hamed, S. Dimopoulos, and G. Dvali, *ibid.* **B436**, 257 (1998); L. Randall and R. Sundrum, Phys. Rev. Lett., **83**, 3370, (1999); L. Randall and R. Sundrum, *ibid.*, **83**, 4690, (1999).
 - [13] J. M. Maldacena, Adv. Theor. Math. Phys. **2**, 231 (1998); E. Witten, *ibid.* 253 (1998); S. S. Gubser *et al.*, Phys. Lett. **B428**, 105 (1998); N. Arkani-Hamed *et al.*, JHEP **0108**, 017 (2001); R. Rattazzi *et al.*, *ibid.* **0104**, 021 (2001).
 - [14] R. Casalbuoni, S. De Curtis, D. Dominici, and R. Gatto, Phys. Lett. **155B**, 95 (1985); Nucl. Phys. **B282**, 235 (1987); R. Casalbuoni, P. Chiappetta, S. De Curtis, F. Feruglio, R. Gatto, B. Mele, and J. Terron, Phys. Lett. **B249**, 130 (1990).
 - [15] M. Gintner, J. Juráň, and I. Melo, Phys. Rev. D **84**, 035013 (2011).
 - [16] M. Bando, T. Kugo, and K. Yamawaki, Phys. Rep. **164**, 217 (1988).
 - [17] R. Contino, T. Kramer, M. Son, and R. Sundrum, J. High Energy Phys. 05 (2007) 074.
 - [18] A. Pomarol and J. Serra, Phys. Rev. D **78**, 074026 (2008).
 - [19] B. Bellazzini, C. Csáki, J. Hubisz, J. Serra, and J. Terning, J. High Energy Phys. 11 (2012) 003.
 - [20] G. F. Giudice, C. Grojean, A. Pomarol, and R. Rattazzi, J. High Energy Phys. 06 (2007) 045; E. Accomando, L. Fedeli, S. Moretti, S. De Curtis, and D. Dominici, [arXiv:1208.0268](#); S. De Curtis, D. Dominici, L. Fedeli, and S. Moretti, [arXiv:1210.7649](#); A. E. C. Hernández and R. Torre, Nucl. Phys. **B841**, 188 (2010); H. S. Fukano and K. Tuominen, [arXiv:1210.6756](#); R. Barbieri, D. Buttazzo, F. Sala, D. M. Straub, and A. Tesi, [arXiv:1211.5085](#); S. Matsuzaki and K. Yamawaki, Phys. Rev. D **85**, 095020 (2012).
 - [21] J. R. Espinosa, C. Grojean, and M. Muehlleitner, EPJ Web of Conf. **28**, 08004 (2012), [arXiv:1202.1286](#); D. Binosi and A. Quadri, [arXiv:1210.2637](#).
 - [22] R. Contino, Y. Nomura, and A. Pomarol, Nucl. Phys. **B671**, 148 (2003); K. Agashe, R. Contino, A. Pomarol, *ibid.* **B719**, 165 (2005).
 - [23] S. Weinberg, Phys. Rev. **166**, 1568 (1968).
 - [24] G. Altarelli, R. Barbieri, and F. Caravaglios, Nucl. Phys. **B405**, 3 (1993); Int. J. Mod. Phys. **A13**, 1031 (1998).
 - [25] E. Malkawi and C.-P. Yuan, Phys. Rev. D **50**, 4462 (1994); **52**, 472 (1995).
 - [26] F. Larios, M. A. Pérez, and C.-P. Yuan, Phys. Lett. **B457**, 334 (1999).
 - [27] H. Georgi, Nucl. Phys. **B361**, 339 (1991).
 - [28] R. D. Peccei and X. Zhang, Nucl. Phys. **B337**, 269 (1990).
 - [29] C. P. Burgess and D. London, Phys. Rev. D **48**, 4337 (1993).
 - [30] E. Accomando, D. Becciolini, S. De Curtis, D. Dominici, and L. Fedeli, Phys. Rev. D **83**, 115021 (2011).
 - [31] E. Accomando, S. De Curtis, D. Dominici, and L. Fedeli, Phys. Rev. D **79**, 055020 (2009); M. Gintner, I. Melo, and B. Trpišová, [arXiv:0903.1981](#); D. Barducci, A. Belyaev, S. De Curtis, S. Moretti, and G. M. Pruna, [arXiv:1210.2927](#).
 - [32] ALEPH Collaboration *et al.*, Phys. Rep. **427**, 257 (2006).
 - [33] K. Nakamura *et al.* (Particle Data Group), J. Phys. G **37**, 075021 (2010).
 - [34] Y. Amhis *et al.* (Heavy Flavor Averaging Group), [arXiv:1207.1158](#).